REPORT DOCUMENTATION PAGE

Form Approved
OMB No. 0704-0188

The public reporting burden for this collection of information is estimated to average 1 hour per response, including the time for reviewing instructions, searching existing data sources, gathering and maintaining the data needed, and completing and reviewing the collection of information. Send comments regarding this burden estimate or any other aspect of this collection of information, including suggestions for reducing the burden, to Department of Defense, Washington Headquarters Services, Directorate for Information Operations and Reports (0704-0188), 1215 Jefferson Davis Highway, Suite 1204, Arlington, VA 22202-4302. Respondents should be aware that notwithstanding any other provision of law, no person shall be subject to any penalty for failing to comply with a collection of information if it does not display a currently valid OMB control number.
PLEASE DO NOT RETURN YOUR FORM TO THE ABOVE ADDRESS.

1. REPORT DATE *(DD-MM-YYYY)*	2. REPORT TYPE	3. DATES COVERED *(From - To)*
03-01-2002	Final	01-11-2000 – 24-11-2001

4. TITLE AND SUBTITLE

Fracture and Toughening of Composites of Polymers and Nanoscale Inorganic and Organic Fillers

5a. CONTRACT NUMBER
F6256200M9202

5b. GRANT NUMBER

5c. PROGRAM ELEMENT NUMBER

5d. PROJECT NUMBER

5e. TASK NUMBER

5f. WORK UNIT NUMBER

6. AUTHOR(S)

Prof. (Neal) Tai-Shung Chung

Prof. Albert F. Yee

7. PERFORMING ORGANIZATION NAME(S) AND ADDRESS(ES)
Institute of Materials Research and Engineering
3 Research Link
Singapore 117602
Singapore

8. PERFORMING ORGANIZATION REPORT NUMBER
N/A

9. SPONSORING/MONITORING AGENCY NAME(S) AND ADDRESS(ES)

AOARD
UNIT 45002
APO AP 96337-5002

10. SPONSOR/MONITOR'S ACRONYM(S)
AOARD

11. SPONSOR/MONITOR'S REPORT NUMBER(S)
AOARD-004016

12. DISTRIBUTION/AVAILABILITY STATEMENT

Approved for public release; distribution is unlimited.

13. SUPPLEMENTARY NOTES

14. ABSTRACT

The objectives of the project were to investigate the mechanical properties and particularly the fracture mechanisms of a number of nanocomposites, and to discover possible approaches to their toughening. The nanocomposites investigated included PA-6/clay (materials supplied by the AFRL) and silsesquioxane-based hybrid materials (supplied by Prof. Rick Laine of the University of Michigan).

The embrittlement of PA-6 nano-clay composites was mainly due to microcracking, followed by global fracture. The toughening-by-bridging approach proved to be somewhat effective. PVDF shows no evidence of plastic deformation, but exhibited good adhesion. Silsesquioxane/epoxy based on octa-cyclohexenyl silsesquioxane epoxide cubes and diaminodiphenyl methane was brittle, but some plastic deformation was observed. Toughening through additions of core-shell rubber particle (up to 4 wt.%) was not very effective. Further study may involve high concentrations of CSR.

15. SUBJECT TERMS

Nanocrystalline Materials, Nanocomposites

16. SECURITY CLASSIFICATION OF:			17. LIMITATION OF ABSTRACT	18. NUMBER OF PAGES	19a. NAME OF RESPONSIBLE PERSON
a. REPORT	b. ABSTRACT	c. THIS PAGE			Kenneth C. Goretta, Ph.D.
U	U	U	UU	40	19b. TELEPHONE NUMBER *(Include area code)* +81-3-5410-4409

IMRE

Fracture and Toughening of Composites of Polymers and Nanoscale Inorganic and Organic Fillers

(Contract Number AOARD-00-4016)

Final Report

For

The Air Force Office of Scientific Research, U. S. A.

Institute of Materials Research and Engineering
3, Research Link
Singapore 117602

24 October 2001

20020129 092

Table of Content

Executive Summary **3**

1 Introduction & Project Objectives **5**

2 Experimental **6**

3 Mechanical Properties **6**

4 Fractographic Analysis **9**

5 Embrittlement Mechanisms **13**

- **i. Extrinsic Factors** **13**
  - a. Degradation of Molecular Weight 13
- **ii. Intrinsic Factors** **16**
  - a. Crystalline Morphology 16
  - b. Crazing 18
  - c. Micro-cracking 20

6. Toughening Through Bridging **23**

- **i. Strategies for toughening** **23**
- **ii. Mechanical Properties** **23**
- **iii. Fractographic Analysis** **25**
- **iv. SAXS Anaylsis** **28**

7. Toughening of Silsesquioxane Epoxy Resin **29**

- **i. Experimental** **29**
- **ii. Effect of DDM Concentration** **30**
- **iii. Effect of Curing Condition** **31**
- **iv. Deformation of OC/DDM Matrix** **32**
- **v. Toughening of OC/DDM Using Core-Shell Rubber** **34**
  - a Deformation behavior of OC/DDM/CSR Composites 35
  - b. Thermal Mechanical Property of OC/DDM/CSR 36
  - c. Compression Test 37
  - d. Fracture Toughness 37
  - e. SEM of CSR modified material 38

8. Conclusions **39**

9. Further Research **39**

Executive Summary

The objective of the project is to investigate the mechanical properties and particularly the fracture mechanisms of a number of nanocomposites, and to discover possible approaches to their toughening. The nanocomposites investigated include PA-6/clay, materials supplied by the AFRL, as well as silsesquioxane-based hybrid materials. The material to be supplied by Dr. Vaia of AFRL was not yet available because of the quantity required for mechanical testing. The silsesquioxane material was supplied by Prof. Rick Laine of U. of Michigan in a collaboration.

I) PA-6/nanoclay composite

PA-6/nanoclay composites have been prepared through melt mixing PA-6 (from Ube) and modified clay (I30TC from Nanocor, USA) using a twin-screw extruder. Under optimum processing conditions the resulting composites exhibited an exfoliated morphology, as confirmed by WAXS and SAXS.

The tensile property and fracture toughness of the composites were studied. The yield stress and tensile modulus increased with modified organic clay concentration as reported in the literature. However the elongation at break decreased dramatically when the clay concentration was higher than 2.5 wt-%; concurrently the fracture toughness also decreased significantly.

Extrinsic vs. Intrinsic Embrittlement Mechanisms. The embrittlement mechanisms of PA-6/nanoclay composites were classified into two categories: *extrinsic* and *intrinsic*. According to this classification degradation of polymer matrix, particle aggregation and processing defects can be regarded as possible *extrinsic* factors, while crystalline morphology, molecular confinement, crazing and micro-cracking are possible intrinsic factors.

The intrinsic viscosity of PA-6/nanoclay composites from melt compounding was comparable to that prepared by physical mixing, thus demonstrating that there was no degradation to contribute to the brittleness of the resulting composites. WAXS indicated that the clay was exfoliated in the polymer matrix, while SAXS showed no significant aggregates up to a length scale of 80 nm, suggesting that aggregation is not a contributing factor to the brittle response of the composites either. We conclude that the embrittlement mechanism is *probably* not due to the extrinsic factors discussed above.

SAXS showed that the addition of clay did not change the lamellar thickness of PA-6 but the lamella population was reduced. Furthermore, SAXS of fractured samples showed that PA-6 containing 2.5 wt-% of nanoclay exhibited high craze concentration, which decreased significantly with increase of clay content (i.e. 5% and 7.5%). Microcracks were formed in the direction parallel to tensile axis. Compared with 2.5% clay composite, the composites containing 5% and 7.5% clay exhibited low concentration of microcracks. The combination of high yield stress and low craze/microcrack concentration suggests that premature breakdown of crazes led to the brittle behavior.

Toughening of PA-6/nanoclay composites. The nature of the embrittlement mechanism led us to attempt to toughen PA-6/nanoclay using the crack bridging mechanism via thermoplastic particles. PVDF was chosen because it is known to adhere to and disperse well in PA-6. A system loaded 10 wt-% PVDF exhibited improved mechanical properties including higher strain to failure and higher toughness. The toughening mechanism is under investigation.

II. Silsesquioxane epoxies (SE)

Silsesquioxane epoxies based on octa-cyclohexenyl silsesquioxane epoxide cubes (OC) and diaminodiphenyl methane (DDM) (from Alfa Aesar) were prepared by Prof. Laine and his student at Michigan for this study. The student also performed all the mechanical studies described in the following under the supervision of AF Yee. The curing condition for the SE system has been studied and optimised. The thermal mechanical property of the resulting SE depends on the curing conditions and the OC/DDM ratio. The SE has high T_g (150°C), good thermal stability (5% weight loss at 410°C). The tensile modulus, up to 3 GPa at room temperature, is typical of conventional epoxies. The fracture toughness, K_{1C}, is in the range of 0.45 to 0.65 MPa-m$^{1/2}$, i.e., they are rather brittle. The capacity of each SE for plastic deformation was assessed using indentation and optical microscopy methods. Extensive plastic deformation was followed by fracture at the tip of the indent. Core-shell rubber (from Prof. Sue of Texas A& M) was used to toughen the epoxy system. Indentation without cracking was observed for SE containing core-shell rubber. The increase of fracture toughness, K_{1C}, however, is rather minimal (~10%).

Conclusion from this Period

The research performed in this period produces two important conclusions:

The embrittlement of normally ductile matrices, at least in the case of PA-6, is not due to extrinsic factors. This is an important conclusion because if extrinsic factors were the cause then the toughening strategy should focus on the elimination of these factors, at least as a first step.

The toughness of PA-6/nanoclay can be partially restored, although this causes the modulus gain to become lost again. However this observation does not necessarily mean that the toughening strategy is ineffective. Rather, a more suitable toughening agent may need to be investigated.

1 Introduction & Project Objectives

The continuing search for high strength-to-weight polymer materials that meet performance requirements for applications under demanding conditions, yet possess reasonable processability, has until recently been focused on fibre reinforced plastics. In the last decade, organic/inorganic nanocomposites have demonstrated exceptional properties that suggest these materials may supplant some traditional composite materials for a wide variety of structural and thermal applications. Nanocomposite materials are composed of two or more phases dispersed over a scale of nanometers. The discovery by researchers at Toyota that exfoliated clay in the form of nanoplatelets, even in very small amounts, can significantly enhance the modulus of polyamide-6 sparked a flurry of activities by nearly every major plastics producer and materials user. In particular, the Toyota researchers discovered that for polymers reinforced with clay, the tensile modulus is typically much greater in nanoscale composites than in corresponding micro-scale composites. The impressive reinforcing effect has never been explained in molecular terms – an absolutely necessary development because of the length scale of the reinforcement materials and because of the way polymer infiltration into the clay is accomplished. On the negative side, it has also been found that nanocomposites are sometimes much more brittle than the pure matrices; at other times the opposite has been found. These apparently conflicting results render a unified molecular-level explanation extremely difficult.

Nanoclay reinforced polymers are just one example of the large variety of new materials with nanoscale fillers and inorganic/organic hybrid materials being developed and investigated. These new materials promise a plethora of interesting properties and new applications. They all need to be mechanically robust, yet many are brittle. This handicap may ultimately prevent a material from being applied regardless of its other merits. The investigation of the origin of the reinforcement effect and the fracture behavior of these materials, and a rational way to toughen them are the motivations for this research.

The objective of the proposed research is to investigate the mechanical properties, and particularly the fracture mechanisms of a number of nanocomposites, and to discover possible approaches to their toughening. Microscopic mechanisms for deformation and fracture will be investigated on several length scales ranging from macroscopic to the nanometer. These mechanisms will be related to the morphology and nanostructure of the materials. On the basis of these mechanisms the morphology and nanostructure of the materials may be modified by material composition, surface treatment, and/or processing in order to promote mechanisms that may intrinsically yield higher toughness. Suitable tougheners will be used to evaluate their effectiveness, and to discover underlying mechanisms.

In this first year progress report, we focus on PA-6 nanoclay systems. We will describe the preparation and characterisation of the microstructure and mechanical behaviour of PA-6 nanoclay composites. We will report our findings on the embrittlement (extrinsic and intrinsic) mechanisms of the composites system and propose a strategy to improve the toughness of the composites. In addition, the deformation behaviour and toughening strategy for silsesquioxane epoxy based on octa-cyclohexenyl silsesquioxane epoxide cubes and diaminodiphenyl methane will also be discussed.

2 Experimental

The polymer matrix used in this study is PA-6 (grade: SF1018A) from UBE. Organoclay fillers (grade: I30TC) were kindly supplied by Nanocor.

The nanocomposites were prepared by melt compounding using a Brabendar twin screw extruder at a processing temperature of 250°C and screw speed of 100 rpm. Prior to processing, PA-6 granules were dried in a vacuum oven at 110°C for two days, and organoclay was dried in an oven at 80°C for 4 hours. The toughened nanocomposites (PA-6-clay-PVDF composite) was prepared by melt compounding of PA-6-clay nanocomposite with PVDF by using a Brabendar twin screw extruder at a processing temperature of 250°C and screw speed of 100 rpm. Prior to processing, PA-6-clay nanocomposites were dried in a vacuum oven at 110°C for two days.

The granules of PA-6-clay nanocomposites or PA-6-clay-PVDF nanocomposites were dried in a vacuum oven at 110°C for two days, and then were injection-moulded to give dog bone tensile bars and bars for Kc tests. Tensile mechanical properties of the nanocomposites were measured by using an Instron machine at a crosshead speed of 5mm/min and room temperature according to ASTM standard D638.

Single-edgenotch bend (SENB) specimens were prepared for the determination of fracture toughness Kc. Specimen thickness (B) and width (W) were 6.35 and 12.7 mm, respectively. For the preparation of a sharp notch in specimens, a razor blade was first immersed in liquid nitrogen until boiling stopped, then was inserted into specimens by tapping with a mallet. Kc was measured by using an Instron machine at a crosshead speed of 5mm/min and room temperature according to ASTM standard D5045. The thickness of the specimens was not large enough to establish true plane strain conditions.

Wide angle X-ray diffraction was performed with a Philips Analytical X-ray (X'Pert) using nickel-filtered Cu-Kα1 radiation source (λ = 0.15418 nm) under a voltage of 45 kV and a current of 40 mA. The XRD patterns were recorded with a step size of 0.05° from 2θ = 2° to 30°. Small angle X-ray scattering was performed on a Burke Nanostar small angle diffractometer. Cu-Kα1 radiation source (λ = 0.15418 nm).

The fracture surfaces was coated with gold and examined using a scanning electron microscope (SEM).

3 Mechanical Properties

The nominal stress-strain curves of the nanocomposites are shown in *Figure 3.1*. Neat PA-6 has the lowest yield stress and largest strain-at-break. For the nanocomposite containing 2.5wt% clay, the yield stress is increased and strain-at-break is sharply decreased. When the clay content in the nanocomposite reaches 5wt%, the yield stress was very close to the fracture stress. However, with a further increase of clay content, no yield took place, and specimens failed at very low strain-at-break values.

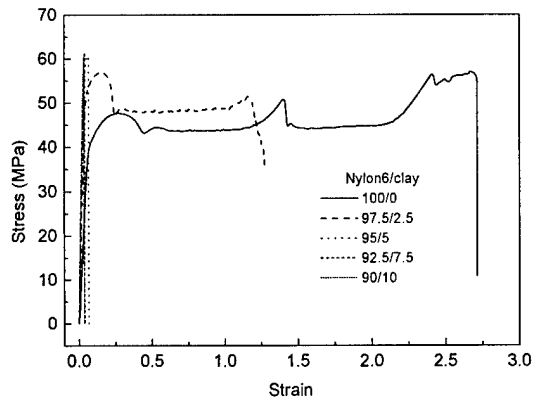

Figure 3.1 Nominal stress-strain curves of PA-6-clay nanocomposites at a crosshead speed of 5 mm/min

The variations of modulus and strain-at-break with clay content are shown in *Figure 3.2*. The modulus of the nanocomposite increases quickly with increasing clay content. The modulus of the nanocomposite containing 5 wt% clay is twice as much as that of neat PA-6. This is a very high stiffening efficiency, which cannot be achieved by conventional glass fibre reinforcement. It is quite certain that clay rather than the crystalline form play a crucial role in the deformation of the nanocomposites. The negative effect on toughness arising from the addition of organoclay overwhelms the positive effect from the crystal transformation of the matrix.

The fracture toughness values of the nanocomposites were measured at a cross head speed of 5 mm/min according to ASTM D5045. For plane strain conditions, the following size criteria must be satisfied:

$$B, a, (w-a) > 2.5\left(\frac{K_Q}{\sigma_Y}\right)^2 \quad ,$$

where B is the specimen thickness, a is the notch depth, W is the specimen width, K_Q is the apparent fracture toughness, and σ_Y is the yield stress of the material under similar conditions.

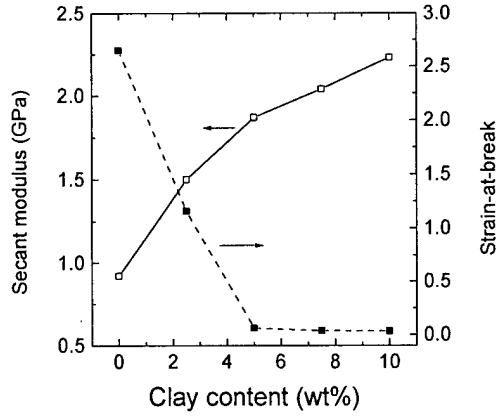

Figure 3.2 Variations of modulus and strain-at-break with clay content for PA-6-clay nanocomposites

B and W in this work are fixed at 6.35 and 12.7 mm, respectively. This geometry satisfies the requirement for the plane strain condition for the PA-6-clay nanocomposites containing 5wt% clay or more. However, the thickness of samples with low content of clay was not thick enough, the effect of plane stress cannot be neglected. Therefore, only the Kc term was used in this work. It is denoted K_{IC} for specimens thick enough and K_Q for specimens not thick enough.

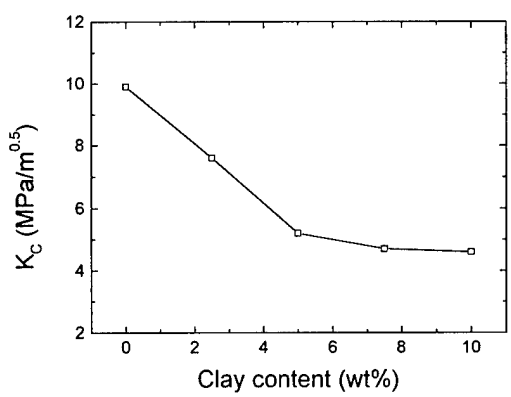

Figure 3.3 Variation of fracture toughness K_c with clay content for PA-6-clay nanocomposites

Figure 3.3 shows that Kc decreases very quickly with increasing clay content in the range from 0 to 5wt%. With a further increase of clay content, the decrease of fracture toughness becomes slow. It is obvious that the fracture toughness of PA-6-clay nanocomposites decreases with increasing clay content. This trend is consistent with that observed in tensile tests.

4 Fractographic Analysis

The fracture surface was observed by using SEM. The observation locations are schematically illustrated in *Figure 4.1*. Location A is close to the razor sharpened notch. Location B is in the middle of the fracture surface. Location C is far from the razor sharpened notch. In general, a crack is initiated at location A, and propagates in locations B and C. The SEM observations at the three locations give an overview of a fracture surface.

Figure 4.2 shows the SEM micrographs of the fracture surface subject to Kc measurements for neat PA-6. At the crack initiation stage, the fracture surface is not very rough (*Figure 4.2A*). At the crack propagation stage, the roughness of the fracture surface (*Figure 4.2B*) is similar to that in 4.2A. However, at the final stage of crack propagation, the fracture surface becomes rather smooth (*Figure 4.2C*).

The surface roughness is roughly indicative of how a crack is initiated and propagated. In general, the greater the surface roughness, the more the volume of matrix involved in deformation, and the higher the fracture toughness. *Figure 4.2A and B* indicate that the crack was initiated and propagated in a very complex way. It branched and increased the volume of deformation in the PA-6 matrix and suggests that the majority of fracture energy was dissipated by the matrix. Nevertheless, at the final stage of crack propagation the crack propagated very rapidly, and only a small amount of fracture energy was absorbed by the matrix. It should be noted that observations by SEM are rarely definitive. More conclusive interpretation of the fracture mechanism would have to await results from optical microscopy on thin sections through the damage zone.

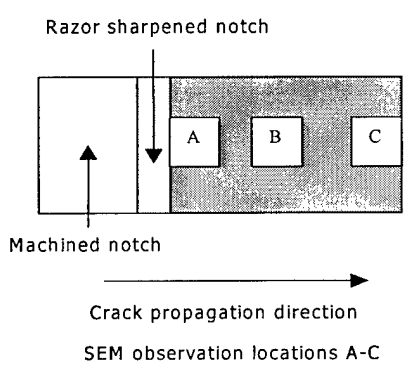

Figure 4.1 Schematic illustration of SEM observation locations A-C on the fracture surface of PA-6-clay nanocomposites

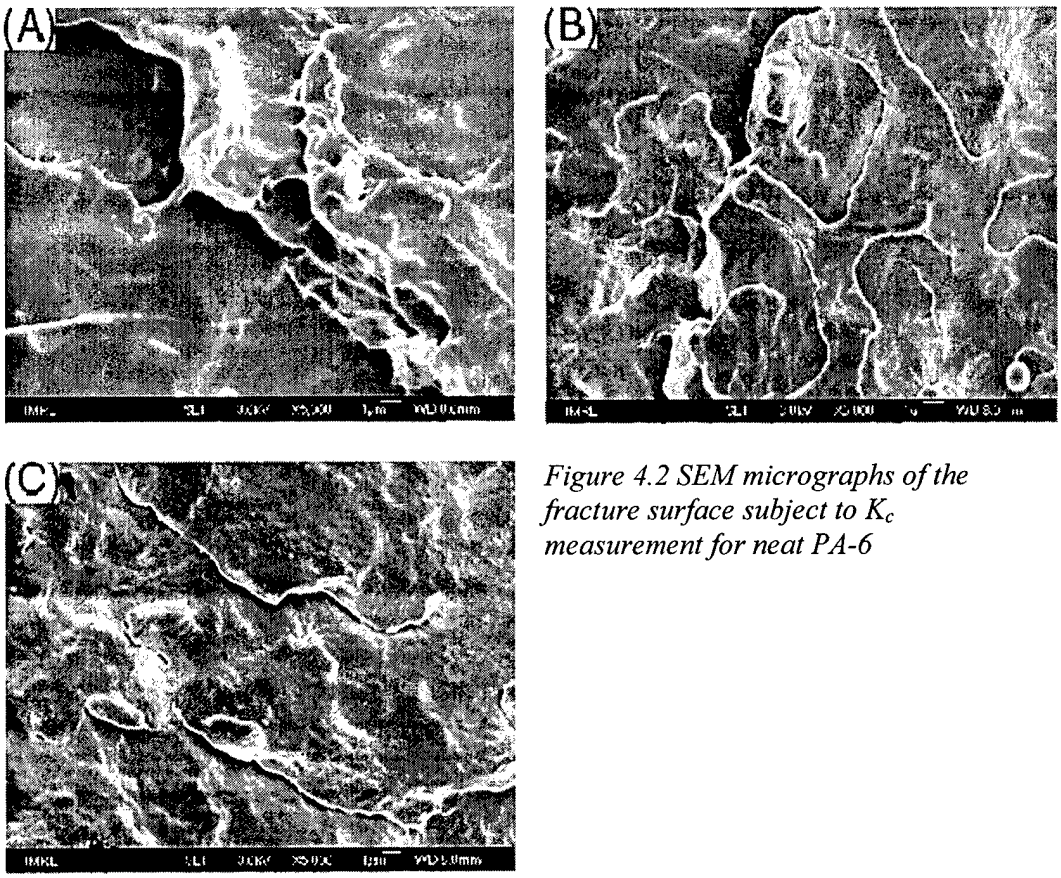

Figure 4.2 SEM micrographs of the fracture surface subject to K_c measurement for neat PA-6

When 2.5wt% organoclay is dispersed uniformly in the matrix, the fracture surface of the nanocomposite is quite different from that of neat matrix. *Figure 4.3A* shows that the fracture surface in this region is very rough. Although such roughness suggests superficial plastic deformation the actual deformation process can be ascertained only by a thorough study of the subsurface damage. By contrast, the fracture surfaces depicted in *Figure 4.3B and C* are very smooth at this scale of magnification. There appears to be roughness on the nm scale. It is tempting to relate this to the presence of the clay platelets but a definitive answer must await further investigation. No large scale plastic deformation is apparent at the two latter locations. Therefore, the majority of fracture energy was probably dissipated at the crack initiation stage. Compared to *Figure 4.2A*, the roughness shown in *Figure 4.3A* is greater. However, the fracture toughness Kc of neat PA-6 is greater than that of the nanocomposite containing 2.5 wt% clay. This is not surprising as SEM micrographs rarely reveal the full spectrum of deformation events in polymers prior to final rupture.

Bubbles and particle clusters may also affect the toughness of polymers. Bubbles can be advantageous or disadvantageous for toughening, depending on many factors, e.g., their size, shape, and concentration. In most cases, particle clusters will decrease toughness. In *Figure 4.3B and C*, no bubbles and clay clusters can be found. This strongly suggests that the clay platelets are well exfoliated in the matrix. If bubbles and clusters are present and have caused premature fracture then they would most likely be observable at the fracture surface. However conclusive evidence for the absence of large defects can only be observed by low magnification microscopy.

None of the techniques employed thus far, viz., SEM and XRD, can rule out the existence of a small number of large defects.

Figure 4.4 is an SEM micrograph of the fracture surface for the nanocomposite containing 7.5 wt% clay. At location A (*Figure 4.4A*), the surface is highly voided. This indicates that clay platelets may have nucleated numerous voids which then grew and coalesced to form a fracture plane. At locations B and C, the fracture surfaces are relatively smooth, and the crack propagated quickly. Therefore, the deformation processes which took place in a volume of material surrounding location A likely absorbed most of the fracture energy. However, the fracture toughness of the nanocomposite containing 7.5 wt% clay is much lower than that of the nanocomposite containing 2.5 wt% clay. This may be due to the formation of the voidy zone which truncated the deformation processes. If this is confirmed to be the case then a lower concentration of clay, or, alternatively, a modification that would increase the cohesive strength of the nanocomposite would increase the toughness.

The appearance of the fracture in 4.4A suggests that the corresponding micrograph for the 2.5 wt% clay is also likely due to voiding followed by void coalescence.

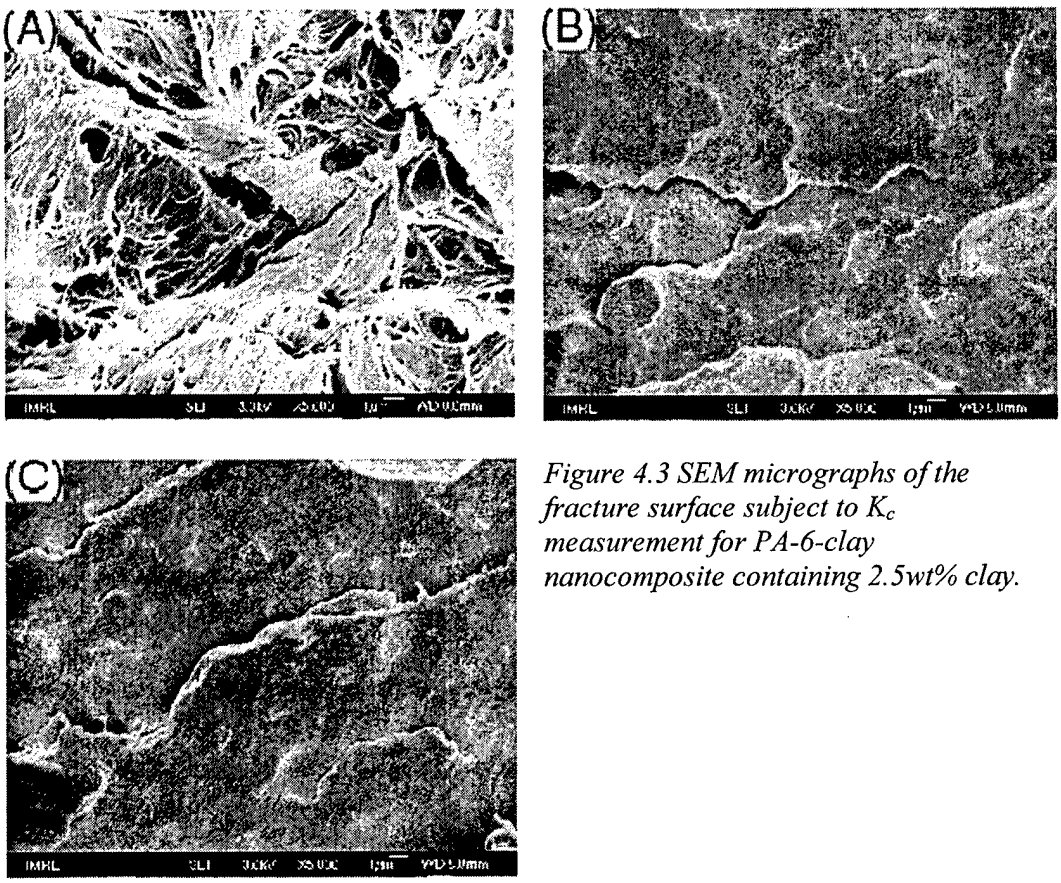

Figure 4.3 SEM micrographs of the fracture surface subject to K_c measurement for PA-6-clay nanocomposite containing 2.5wt% clay.

The clay particles, with a dimension of ca. 100-500 nm, are also observed to uniformly disperse in the matrix, although the clay platelets of ca. 1 nm in thickness cannot be seen. In other words, there may be roughly two types of dispersion of organoclay. A clay particle should consist of a number of stacked nanoplatelets with

an interlayer spacing that is too large for the XRD measurement. It is reasonable to assume that particle size, size distribution, particle spatial distribution and interparticle distance could have substantial influence on toughening. Furthermore, it has been reported that SiO2 nanospheres can effectively toughen PA-6. Thus the size of clay clusters described in this work has the potential of being suitable for toughening.

At location 4.4B, voids observed most likely arise from debonding at the PA-6-clay interface. This hypothesis is based on the assumption that the interfacial adhesion between PA-6 and organoclay is not strong enough to resist debonding. Our hypothesis is clearly different from the notion, advanced by some researchers, that the interaction between PA-6 and clay is strong enough to resist debonding at their PA-6 interface.

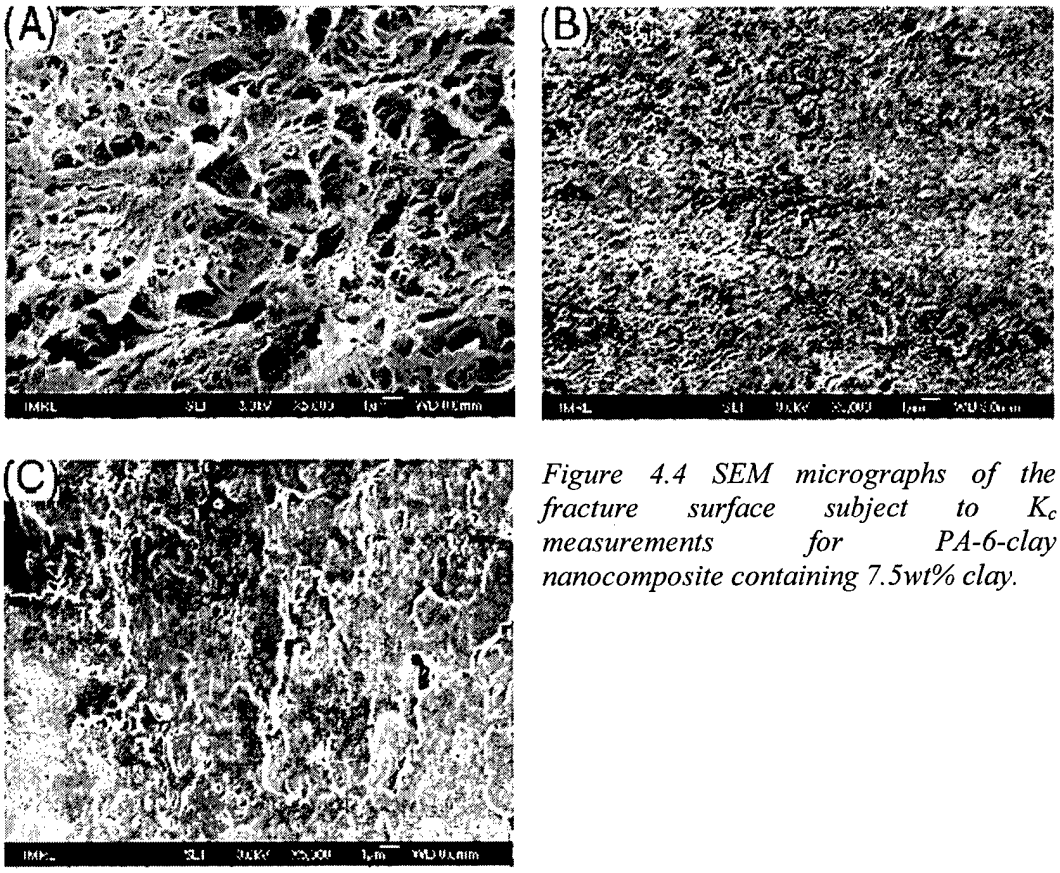

Figure 4.4 SEM micrographs of the fracture surface subject to K_c measurements for PA-6-clay nanocomposite containing 7.5wt% clay.

In summary, SEM micrographs suggest that on the whole the clay platelets are completely exfoliated in the matrix for the nanocomposites containing low concentrations of clay, and but that there are clay clusters in the matrix for the nanocomposites containing high concentrations of clay.

A very strong stiffening effect has been observed with the nanocomposites containing low concentrations of clay. The modulus of the nanocomposite containing 5 wt% clay doubles that of neat PA-6. However, the strain-at-break and fracture toughness of the nanocomposites decrease sharply with increasing clay content.

5 Embrittlement Mechanisms

Many factors could lead to the brittle response of the PA-6 nanoclay composites. They can be classified into two major categories: namely, extrinsic and intrinsic factors. The extrinsic factors, such as degradation of polymer matrix, aggregation of clay and air bubble, etc., may result from the processing of nanocomposites. The intrinsic factors, such as crystalline morphology, confinement, crazing and micro-cracking, are mainly due to the intrinsic change of morphology when nanoclay is incorporated. In the following discussion, these embrittlement mechanisms will be addressed.

i. Extrinsic Factors

a. Degradation of Molecular Weight

Most mechanical properties of a polymer strongly depend on the molecular weight of the polymer, and the brittle response of a polymer material could be an indication of low molecular weight. It has been asserted that incorporating modified clay into a polymer matrix through melt compounding at high temperature (~250°C), could cause degradation catalysed by the addition of clay. The yellowish appearance of the resulting nanoclay PA-6 composites may be another hint for possible polymer degradation.

In order to address this issue, molecular weights of PA-6 containing 5% of clay through melt compounding and through physical mixing were determined and compared with neat nylon. It is found that the molecular weight of the polymer matrix is hardly changed after melt compounding, as shown in table 5.1.

Table 5.1 Effect of Melt Compounding on the Molecular Weight

Polymer systems	Intrinsic viscosity [η]	Molecular weight
PA-6 melt compounding with 5% clay	0.81	19,000
PA-6 physically mix with 5% clay	0.83	19.400
Neat PA-6	0.82	19,200

**Viscosities were determined 25 ℃. Solvent: Formic acid*

It is clear that in the system studied here, the melt compounding does not lead to thermal degradation of the polymer matrix.

b. Aggregation of Clay

Aggregation of clay is also a possible factor that could lead to a brittle response. A homogeneous dispersion of clay on the nano-scale is desired for nanocomposites as it could greatly enhance the mechanical property of the resulting composites. However, if the clay is not exfoliated and forms aggregates in the polymer matrix, these defect-like aggregates would lead to critical stress concentrations and premature failure.

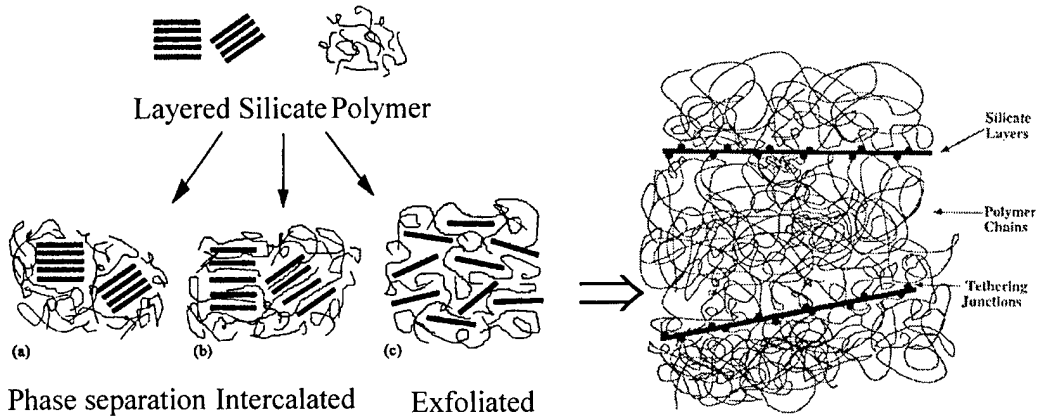

Figure 5.1 Morphology of PA-6-Clay Composites

Wide-angle x-ray scattering and small-angle x-ray scattering are important tools to probe the morphology of nanoclay-composites. The structure of clay resembles a smectic arrangement, where the nanoplatelets are organised in a layer packing arrangement as shown in *Figure 5.1*. This layer arrangement gives rise to low angle scattering in WAXS due to inter-layer distance. As shown in *Figure 5.2*, the WAXS of clay exhibits a peak at about 7° (2θ). When the clay was modified with organic surfactants, the inter-layer distance increases due to the penetration of the quartenary salt into the gap between the layers. As a result, the low angle scattering peak shifts to even lower angles at about 4° (2θ), indicating an intercalated morphology. When the modified clay was melt-mixed with PA-6 using a twin-screw extruder, the scattering peak at 4° (2θ) disappeared. This is a good indication of the successful exfoliation of modified clay. For the polymer systems studied here, i.e., PA-6 containing 2.5%, 5%, 7.5% and 10% of clay, WAXS indicated that the clay has been exfoliated, as shown in *Figure 2*.

Quite often, WAXS is used as an indication of whether clay has been exfoliated. There are however some limitations to this method. First, the clay may still exhibit an intercalated morphology with a longer inter-layer distance that could not be accessed by WAXS since WAXS is normally limited to about 2° (2θ). Second, there is a possibility that the scattering peak due to the intercalated clay (modified clay) disappears yet the clay still exhibits an aggregate morphology. This may occur when the shearing force disrupts the layer packing arrangement during compounding but

does not fully disperse the aggregated clay. One way to address this problem is to use small-angle x-ray scattering which can probe a longer length scale.

Figure 5.3 is the SAXS of PA-6 containing 2.5% of clay. The scattering pattern is dominated by a peak at q ~ 0.08 Å-1 ($q = 4\pi\sin\theta/\lambda$) which corresponds to a *d* spacing of 8 nm. This scattering is probably from the crystalline lamellar structure and the position of the peak represents the lamellar thickness. Except for this peak, there is no significant scattering up to 80 nm. Visual inspection revealed no significant aggregation of large clay particles or moulding defects.

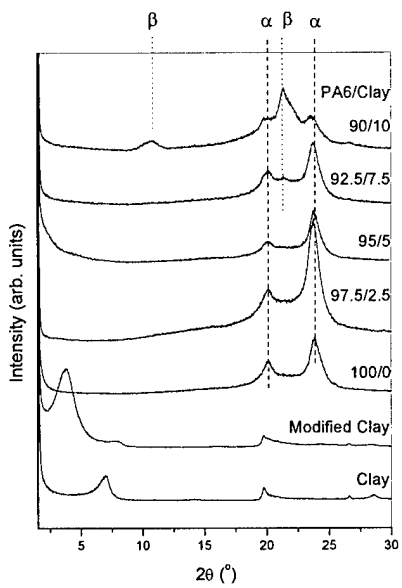

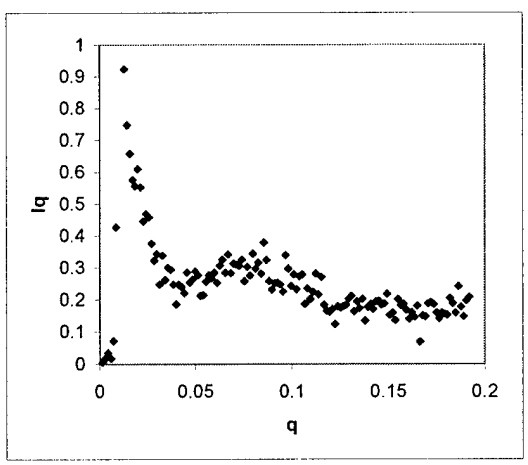

Figure 5.3 Small Angle X-ray Scattering of PA-6 containing 2.5% of clay

Experiment was performed on a NanoStar small angle X-ray diffractometer. Cu Kα: λ=1.5418 Å

No aggregates up to the size of 80nm; Scattering at 8nm attributable to lamellar thickness of PA-6

Wide angle X-ray scattering indicates that the clay is exfoliated in the polymer matrix and Small angle X-ray scattering shows no significant concentration of aggregates up to the length scale of 80 nm. As a result, we do not think aggregation is a contributing factor to the brittle response of the composites.

In summary, extrinsic factors, such as molecular weight degradation and aggregation of clay, are most likely not the contributing factors to the embrittlement phenomenon. However the most definite result, which could be obtained from optical microscopy, has not yet been obtained.

ii. Intrinsic Factors

a. Crystalline Morphology

Crystalline morphology such as crystal structure, crystallinity and the lamellar structure can play significant roles in influencing the deformation behaviours of semi-crystalline polymer composites. Deformation of semi-crystalline polymers occurs first in the amorphous phase, while crazing normally occurs in the region between the two neighbouring lamellae. Addition of clay into PA-6 not only could alter the crystal structure, but also could affect the crystallinity and the population of the lamellae, which would affect the subsequent deformation behaviour of the resulting composites. It is therefore not surprising that it has been reported that PA-6, which is dominated by gamma crystal structure, deforms differently compared with PA-6 with alpha crystals.

Crystal Structure and Crystallinity

PA-6 is a semicrystalline polymer with a rather complex crystalline structure. Nylon-6 is known to exhibit three crystalline forms that coexist in various fractions. The stable monoclinic α form has a planar zig-zag chain conformation, with the H-bonds lying between antiparallel chains in (002) planes. The monoclinic γ form has a chain twist in the amide groups with respect to the methylene segment so that the monomer unit is in a T_4STS (T=trans; S=skew) conformational sequence that slightly shortens the crystallographic chain axis. The H-bonds link parallel chains within (200) planes, and the H-bonded sheets display a regular up and down displacement. The metastable pseudo hexagonal β form is not as well identified, which can be viewed as an intermediate structure between α and γ forms from the standpoint of H-bond setting and chain conformation.

A silicate-induced crystal transformation from the α-form to the γ-form of PA-6 is observed by XRD (figure 5.2), i.e., the formation of γ-form crystals is strongly enhanced by the presence of inorganic fillers. With the increase of clay concentration, the population of γ crystal increases while the population of α crystal decreases. Moreover, the crystallinity of the nanocomposite decreases with the increase in clay concentration, as shown in figure 5.2.

The crystalline form has a great influence on the deformation behavior of neat PA-6. The α form gives rise to a higher stiffness and lower ductility than the γ form. For instance, the yield stress of PA-6 mainly containing the α form crystals is ca. 40 MPa while it is ca. 20 MPa for PA-6 mainly containing the γ form crystals.

The addition of nano-sized clay platelets in the nanocomposites favors the formation of the γ form. Therefore, the stiffness of nanocomposites would decrease

while the ductility would increase with increasing clay content. However, the actual situation that takes place in PA-6/clay nanocomposites is just the opposite.

The nominal stress-strain curves of the nanocomposites are shown in *Figure 3.1*. Neat PA-6 has the lowest yield stress and largest strain-at-break, though it has the highest content of α form crystals. For the nanocomposite containing 2.5wt% clay, the yield stress is increased and strain-at-break is sharply decreased, though the content of γ form crystals is increased. When the clay content in the nanocomposite reaches 5 wt%, the yield stress was very close to the fracture stress. However, with a further increase of clay content, no yield took place, and specimens were fractured at very low strain-at-break values. It is obvious that clay rather than the crystalline form plays a decisive role in the deformation of the nanocomposites. The negative effect on toughness arising from the addition of organoclay overwhelms the positive effect from the crystal transformation of the matrix.

Lamellar Morphology

The result from a SAXS study of the nanoclay composite is shown in figure 5.4. The dominant feature is a peak at about q ~ 0.08 $Å^{-1}$.

This peak most likely represents the lamellar thickness of the polymer matrix. The peak position is almost the same for the neat PA-6 and PA-6 nanoclay composites, indicating that the lamellar thickness does not change with the incorporation of nanoclay. This in turn suggests that clay is mainly distributed in the amorphous part of the composites. The peak intensities for the three polymer systems are, however, different. With the increase in clay content, the scattering intensity decreases, which indicates a reduction in lamellae population.

The reduction in lamellae population may affect the deformation behaviour of semi-crystalline polymers. It is known that crazes are normally initiated between two adjacent lamellae. The decrease of lamellae population could lead to a reduction in tie molecules and hence the propensity to crazing. In the following section, we describe our discovery that craze concentration decreases dramatically with the increase in clay content and the nanocomposite becomes brittle.

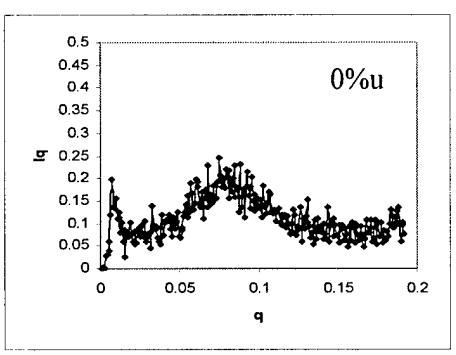

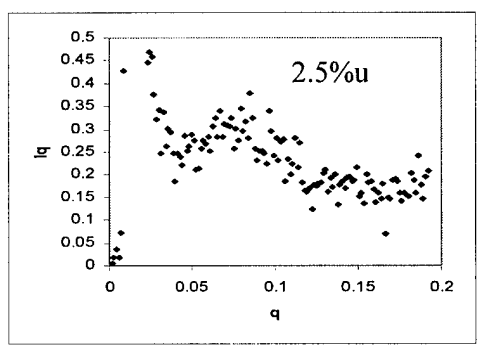

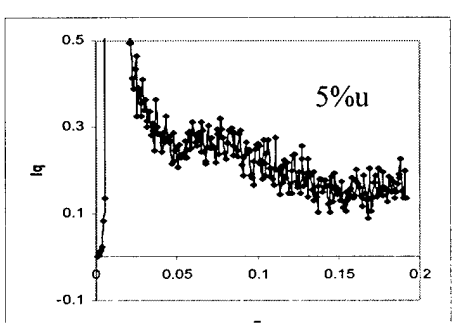

Figure 5.4 SAXS of Nanocomposites

The thickness of sample under X-ray irradiation is roughly the same. No change in lamellar thickness; Lamellae population decreases with increase of clay content

b. Crazing

Crazing could be a mechanism for energy dissipation and a cause for polymer failure. If a polymer system could generate massive crazing during deformation, it may lead to a high level of toughness since the massive crazes would help to dissipate energy. On the other hand, crazes could also lead to premature failure, in particular when a system generates a small amount of crazes; the polymer system would fail due to premature breakdown of one or a few crazes.

Many methods could be used to probe the craze morphology of polymers. TEM is a frequently used method to directly image the craze morphology. The disadvantage of using TEM is that it involves tedious sample preparation and possible artefacts induced during sample preparation. Small angle x-ray scattering is a more effective method to probe the craze morphology. Sample preparation is simple and the information obtained represents an average of a significantly large volume, typically in 105 □m3. Moreover, the concentration of crazes can be determined quantitatively using invariant analysis. In our research, SAXS is used to probe the craze morphology of a fractured polymer sample.

Small Angle X-ray Scattering from Crazes

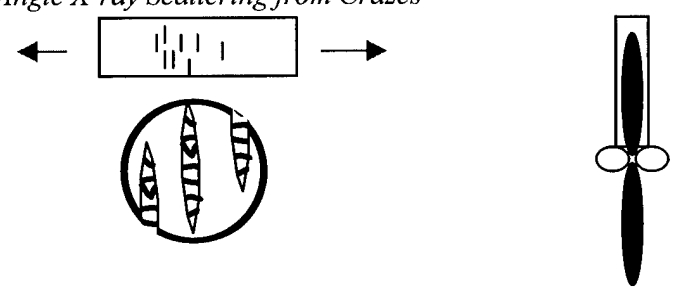

Morphology of Craze **SAXS Signature**

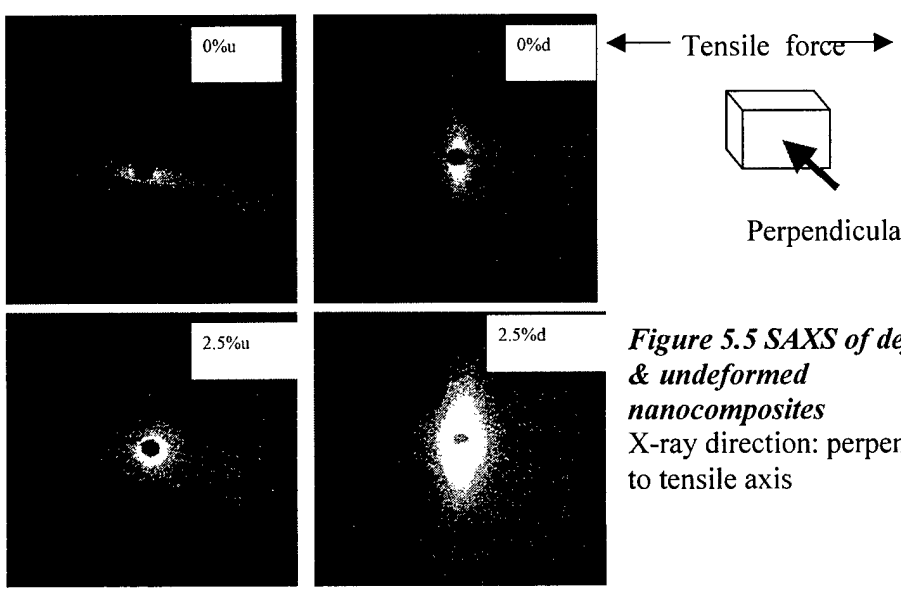

Figure 5.5 SAXS of deformed & undeformed nanocomposites
X-ray direction: perpendicular to tensile axis

As shown in the figure above, if the tensile deformation direction is horizontal, the SAXS from crazes resembles a strip. The meridional scattering is attributed to scattering from fibrils of the crazes, which can be quantitatively related to craze concentration through invariant analysis. Equatorial scattering is hardly seen and could be related to the scattering from the interference of polymer matrix and the crack. Based on this principle, we can study the fracture morphology of polymer composites and probe the possible formation of crazes during deformation.

For neat PA-6, SAXS detects a small amount of crazes after yield. For PA-6 containing 2.5% of clay, the craze concentration is significantly higher as shown in figure 5.5. When integrating the scattering intensity along the meridian as shown in figure 5.6, the intensity for PA-6 containing 2.5% clay is about 40 times that of neat PA-6. This is probably because clay acts as craze nucleation sites, which facilitates the formation of crazes. On the other hand, the increase of yield stress upon incorporating clay also promotes crazing. Due to formation of massive crazes, the PA-6 containing 2.5% clay exhibits high yield stress and tensile modulus, reasonable elongation at break (~100%), and a toughness K_c of ~ 8 MPa-m$^{1/2}$.

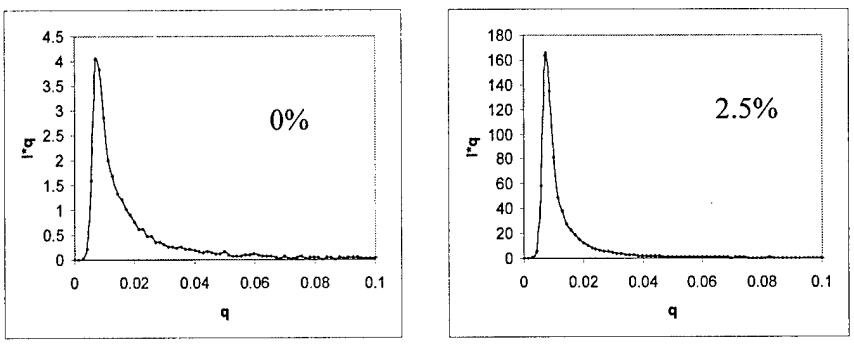

Figure 5.6 SAXS from Crazes (Meridional Scattering)

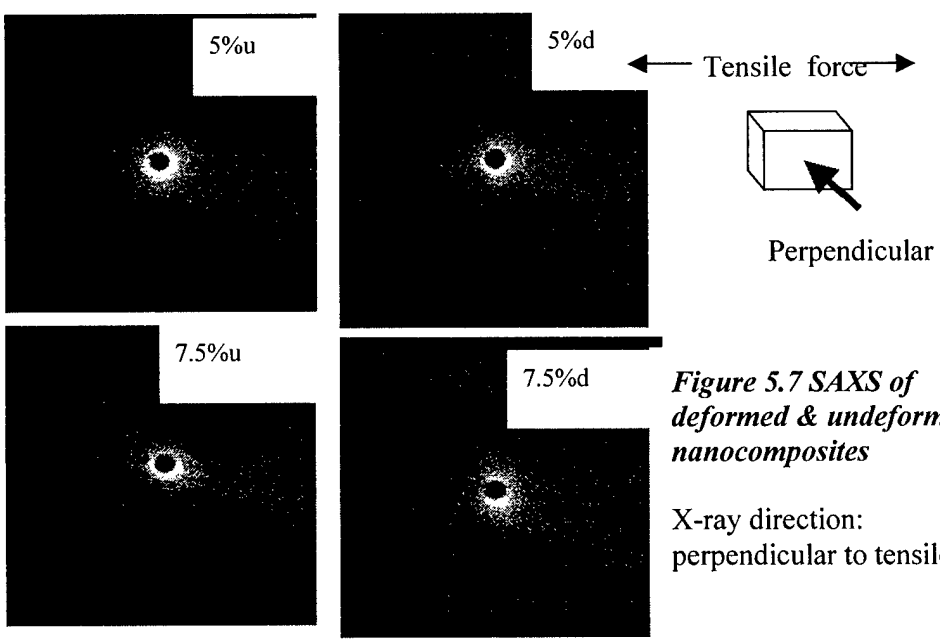

Figure 5.7 SAXS of deformed & undeformed nanocomposites

X-ray direction:
perpendicular to tensile axis

When the clay concentration increases further, i.e. to 5% and 7.5% clay, the materials fail without generating significant crazing. SAXS hardly registers any craze signature, as shown in figure 5.7. By integrating the scattering signal along the meridian as shown in figure 5.8, we can see that the scattering intensity is comparable to the undeformed samples and the intensity is only a small fraction (1%) of that in PA-6-2.5% clay composite.

SAXS clearly indicates that no crazing occurs in the deformation of nanocomposites containing 5% and 7.5% of clay, in contrast to the nanocomposite containing 2.5% clay. These two nanocomposites are also very brittle compared with neat PA-6 or PA-6-2.5% clay composite. The elongation at break for the two composite is lower than 10% while the toughness of the two composites, K_c, are also low. The conclusion on deformation appears highly dependant on filler content.

The fracture behaviour of the nanocomposites correlates well to the fracture morphology of the composites. It seems that the formation of massive crazes may be an important contributor to the toughness of this material.

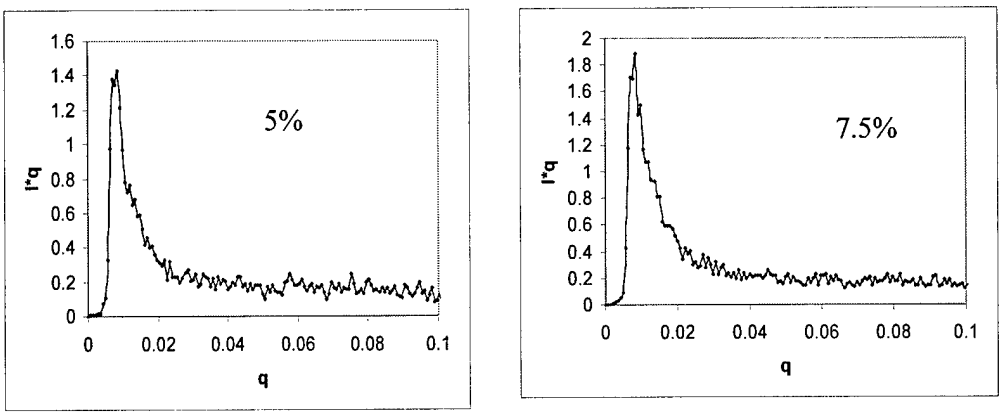

Figure 5.8 SAXS from Craze (Meridional Scattering)

c. Micro-cracking

Similar to crazing, micro-cracking is a mechanism for energy dissipation as well as failure. However, cracks are very difficult to detect using SAXS as the length scale of the crack is well in excess of the ability of our SAXS apparatus to detect, which is limited to about 80 nm. In a synchrotron radiation source using a proper detector set up, the upper limit may be up to 200 nm. Nevertheless, if the crack width is small or the crack is not yet well developed, it may be probed by SAXS. The characteristic of the micro-crack would manifest itself in SAXS as equatorial scattering. The following figure illustrates a typical pattern of cracks and the SAXS pattern expected.

For a polymer under tensile strain, micro-cracks may open up in the direction perpendicular to the tensile axis. If the crack width is not too large it may give rise to small angle scattering. This scattering should be equatorial which would result from density fluctuation between the polymer matrix and the crack width (air). The length scale along the micro-crack propagation direction normally is too big to be detected by SAXS. Equipped with this principle, we can now examine the SAXS from fractured samples.

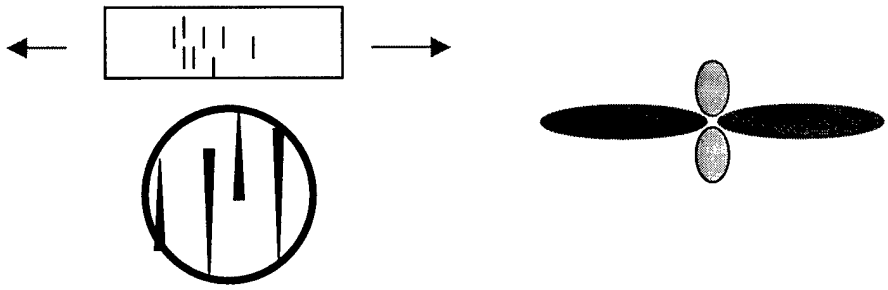

Micro-crack Morphology *SAXS Signature*

Fractured samples were studied in the direction perpendicular and parallel to the tensile axis using SAXS and the results are summarized in figure 5.8. The scattering in the direction perpendicular to the tensile axis has been discussed previously. It represents scattering from crazes in the polymer samples. We however cannot detect any significant micro-cracks in this direction, as the scattering is mainly concentrated on the meridian. A surprising result is that in the direction parallel to the tensile axis, SAXS indicates equatorial scattering with reasonable intensity for nanocomposites containing 5% and 7.5% clay. The SAXS scattering for the nanocomposite containing 2.5% clay in the direction parallel to the tensile axis is so intense that the image cannot be recorded safely in our system. As a result, the data for this composite is not listed here. For neat PA-6, there is not such equatorial scattering. The intensity of equatorial scattering for nanocomposites containing 5% and 7.5% clay is shown in figure 5.9.

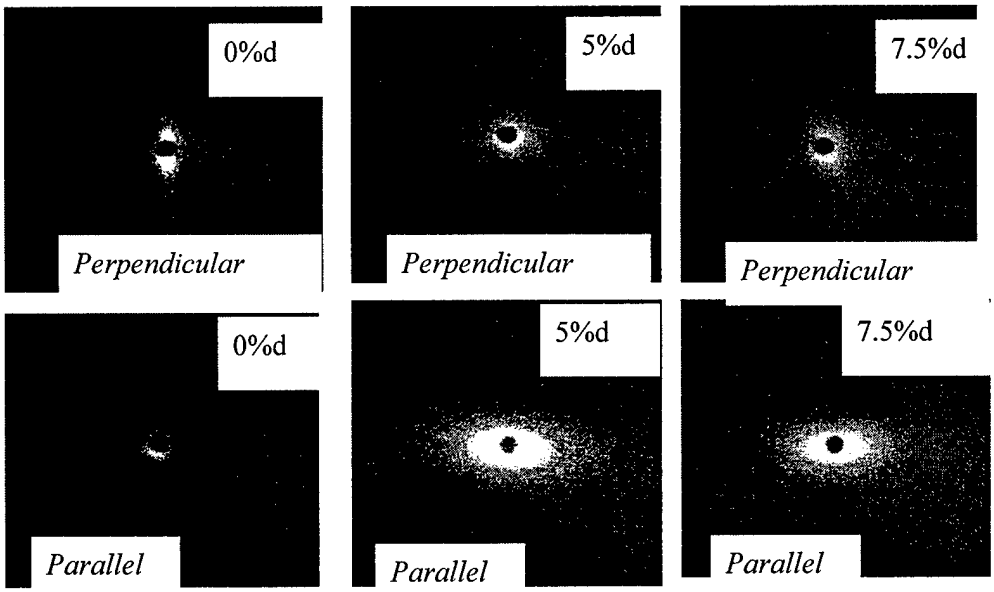

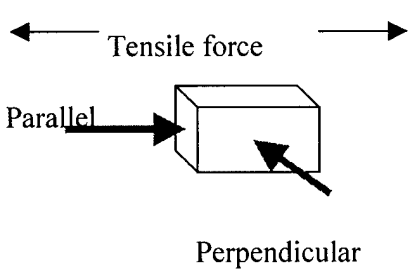

Figure 5.8 SAXS of fractured Nano-composites in different directions.

The nanocomposite containing 2.5% clay is not shown here, as the intensity is too high in the parallel direction.
The result indicates micro-cracking in the direction parallel to tensile axis

The equatorial scattering suggests the existence of density fluctuation along the thickness direction. This scattering is possibly a result of micro-cracking in the polymer samples. Clearly, the appearance of equatorial scattering can be attributed to the addition of clay which induces micro-cracking. Moreover micro-cracking likely occurs in the interface between the polymer matrix and the exfoliated clay, because for neat PA-6 there is no such equatorial scattering, even though SAXS detects crazes in the sample. This is understandable, as clay is exfoliated; during the injection molding process, the exfoliated clay nano-plates may orient in the direction of the flow (the same as the tensile direction) due to the highly anisotropic shape of the platelets. When the tensile bar is subjected to tensile strain, a weak interface between the matrix polymer and the exfoliated clay may initiate micro-cracking which would give rise to equatorial scattering.

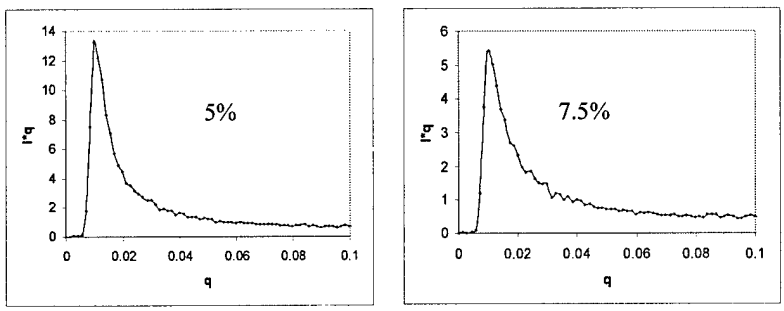

Figure 5. 9 SAXS from Micro-Cracks (Equatorial Scattering)

Summary

Having studied the morphology and deformation behavior of this series of nano-composites, several conclusions may be drawn. First, addition of clay to PA-6 affects the type of crystal structure and also crystallinity. It does not affect the lamellar thickness but reduces lamellae population. These will also affect the subsequent deformation. Second, under tensile deformation, the nanocomposite containing 2.5% clay exhibits massive crazes and massive micro-cracks while nanocomposites containing 5% and 7.5% clay exhibit little crazing but instead a small amount of micro-cracking. As a result, the nanocomposite containing 2.5% clay has better mechanical properties than those nanocomposites with 5% and 7.5% clay. These results suggest that massive crazing and massive micro-cracking in PA-6 nanoclay composites are beneficial. Third, the brittle response for nanocomposites with 5 and 7.5% of clay can be attributed to the existence of a small amount of micro-cracks in the samples. Two approaches may be applied to toughen these nano-composites: i) using crack bridging method to delay the development of cracks; ii) using particles, such as rubber particles, to induce mass crazes.

6. Toughening Through Bridging

i. Strategies for toughening

Fracture energy can be absorbed either by matrix shear yielding or by particle bridging a crack. In this part of the work we attempt to toughen the nanocomposites using bridging particles. A number of criteria are essential for this mechanism to be effective. For instance, the interfacial adhesion must be strong enough to allow the bridging mechanism to take effect. Another requirement is that the bridging particles are large compared to the intrinsic size of the crack tip process zone. A third criterion is that the bridging particle is capable of substantial plastic deformation. This would suggest the use of crystalline thermoplastic materials. We begin our exploration by identifying thermoplastic particles that would adhere well to our matrix.

It has been reported that there are specific intermolecular interactions between amide groups along the polyamide chain and F-atoms on PVDF, which are responsible for the very strong interfacial adhesion between the two polymers. In this study, PVDF is tentatively used to toughen PA-6-clay nanocomposites. Figure 6.1 shows the fracture surface of a PA-6-clay-PVDF ternary nanocomposite containing 20 wt% PVDF. A great number of fibrils are seen bridging the PA-6 matrix and PVDF particle, though debonding at interface clearly took place.

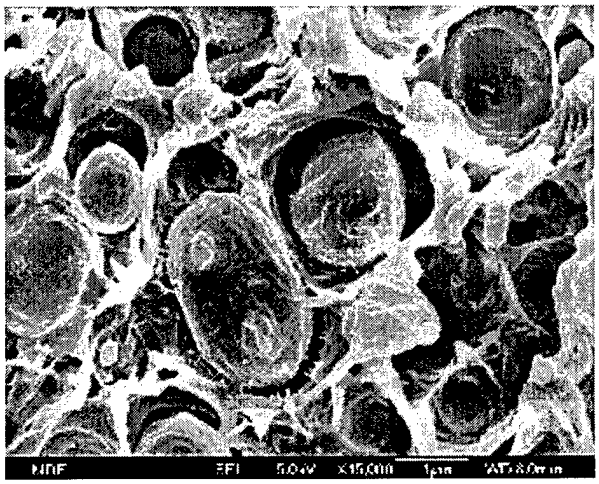

Figure 6.1 SEM micrograph of the fracture surface subject to K_c measurements for PA-6-clay-PVDF ternary nanocomposite containing 20 wt% PVDF

ii. Mechanical Properties

The weight ratio is kept at 95 PA-6/clay for all nanocomposites studied here. The concentration of PVDF is based the overall weight of the three components. The nominal stress-strain curves of the PA-6-clay-PVDF nanocomposites are shown in *Figure 6.2*. All three nanocomposites can yield in tension. However, addition of PVDF does not always reduce the yield stress of nanocomposites. The yield stress of PA-6-clay-PVDF nanocomposite containing 10 wt% PVDF is in fact higher than that

of PA-6-clay nanocomposite. But the yield stress of PA-6-clay-PVDF nanocomposite containing 20 wt% PVDF is lower.

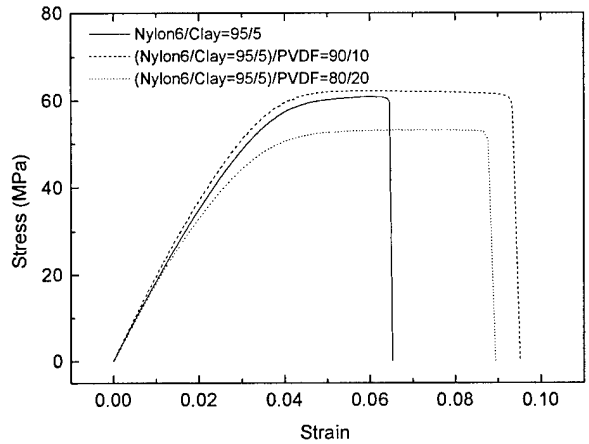

Figure 6.2 Nominal stress-strain curves of PA-6-clay-PVDF ternary nanocomposites containing different concentrations of PVDF. The weight ratio of PA-6 to clay is fixed at 95 to 5

Figure 6.3 plots the modulus and strain-at-break vs. PVDF content. It is obvious that PVDF can be used to toughen PA-6-clay nanocomposites. It is seen that PA-6-clay nanocomposite has the smallest strain-at-break. But the strain-at-break does not always increase with increasing PVDF content. The PA-6-clay-PVDF nanocomposite containing 10 wt% has a slightly larger strain-at-break value than the one containing 20 wt% PVDF. This result may be due to the large uncertainty commonly observed in strain to break values.

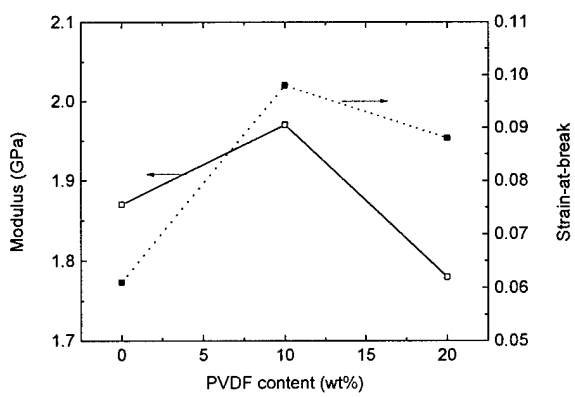

Figure 6.3 Variations of modulus and strain-at-break of PA-6-clay-PVDF ternary nanocomposites with PVDF content. The weight ratio of PA-6 to clay is fixed at 95 to 5

Figure 6.4 plots the of fracture toughness Kc of the nanocomposites vs. PVDF content. The fracture toughness Kc increases with increasing PVDF content. The dependence of fracture toughness Kc on PVDF content is not the same as that of strain-at-break on PVDF content. Compared with the nanocomposite without PVDF, the nanocomposite containing 10wt-% is stiffened and toughened simultaneously. The reason for the unexpected result needs further investigation.

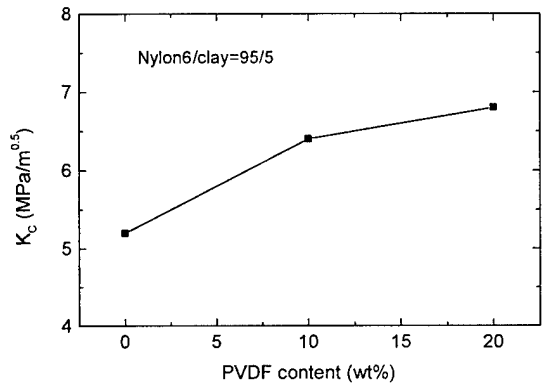

Figure 6.4 Dependence of fracture toughness K_c of PA-6-clay-PVDF ternary nanocomposites on PVDF content. The weight ratio of PA-6 to clay is fixed at 95 to 5

iii. Fractographic Analysis

The fracture surface was observed using SEM. The observation locations are schematically illustrated in *Figure 6.5*. Location A is close to the razor-sharpened notch. Location B is in the middle of the fracture surface. Location C is far from the razor sharpened notch. In general, a crack is initiated at location A, and propagates to locations B and C. The SEM observations at the three locations give an overview of a fracture surface.

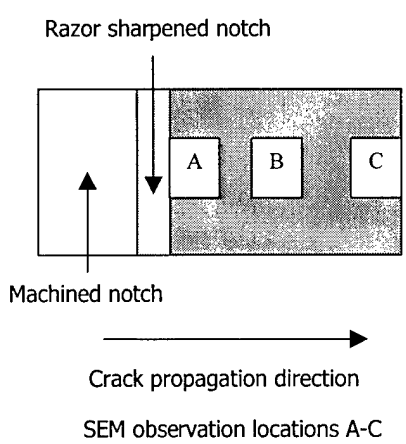

Figure 6.5 Schematic illustration of SEM observation locations A-C on the fracture surface of PA-6-clay nanocomposites.

Figure 6.6 shows the SEM micrographs of the fracture surfaces in PA-6-clay nanocomposite containing 5 wt% clay. Plastic deformation, which probably resulted from the coalescence of voids, is observed at the crack initiation stage at location A close to the razor-sharpened notch (Figure 6.6A). However, it disappeared in the crack propagation stage at locations B (Figure 6.6B) and C (Figure 6.6C). Results reported elsewhere in this report showed that clay platelets were exfoliated in the nanocomposite, as revealed by X-ray diffraction. No clay clusters can be seen from Figure 6.6B and C. Therefore, we conclude that clay platelets are well dispersed in the PA-6 matrix.

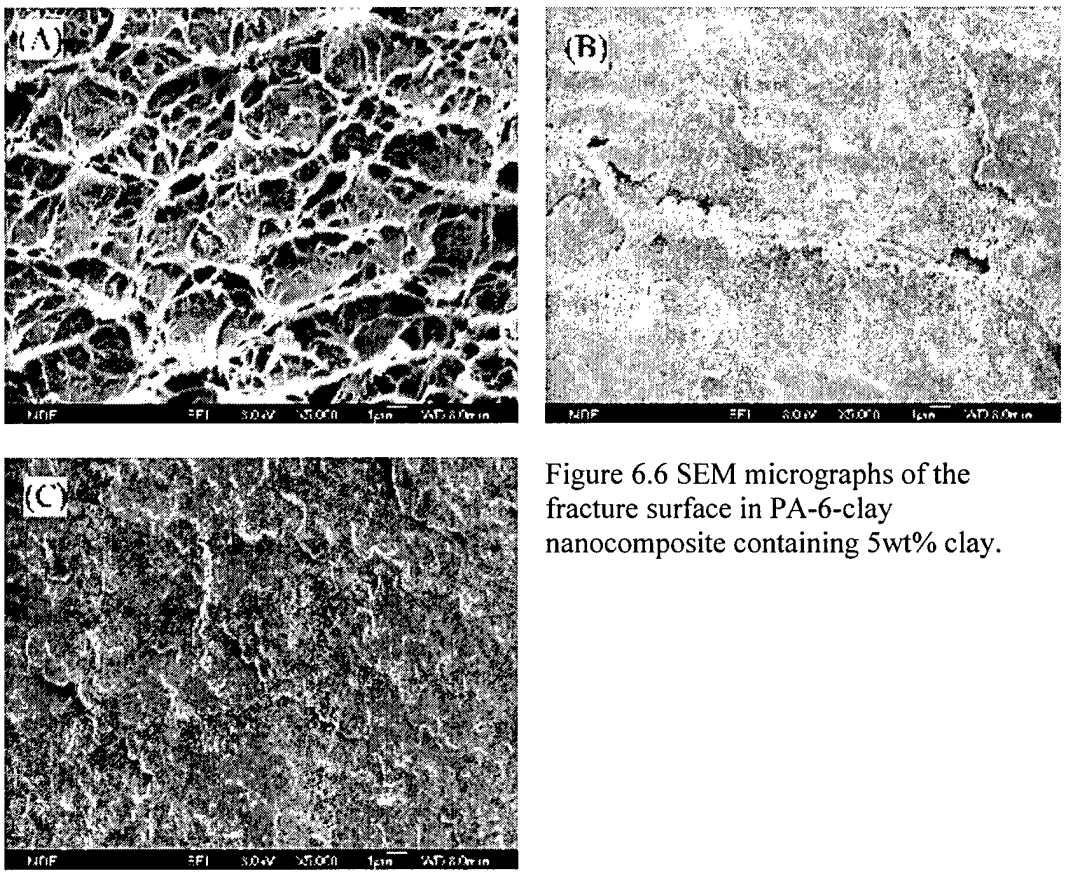

Figure 6.6 SEM micrographs of the fracture surface in PA-6-clay nanocomposite containing 5wt% clay.

Figure 6.7 shows the SEM micrographs of the fracture surfaces in PA-6-clay-PVDF ternary nanocomposites containing 10 wt% PVDF. Plastic deformation of the matrix is also observed at the crack initiation stage at location A close to the razor-sharpened notch (*Figure 6.7A*). But it is less extensive than that observed in *Figure 6.6A*. Like the 5% case the plastic deformation is probably the result of void coalescence. Since the voids undoubtedly grew from the PVDF particles the higher volume fraction of such particles means that the voids do not need to grow much before they coalesce into a crack. The plastic deformation disappeared at the crack propagation stage at locations B (*Figure 6.7B*) and C (*Figure 6.7C*). PVDF particles around 0.5μm are seen in this figure. Debonding at the PA-6-PVDF interface is observed. Some PVDF particles were also detached from the fracture surface.

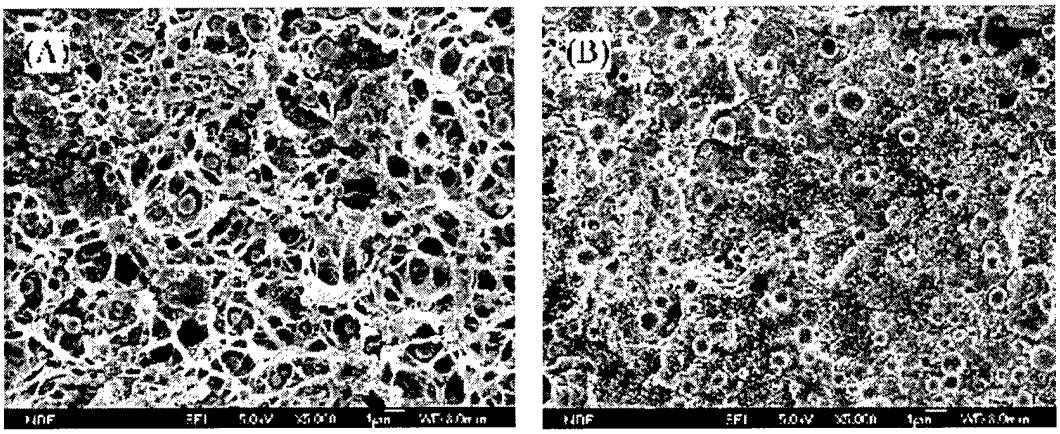

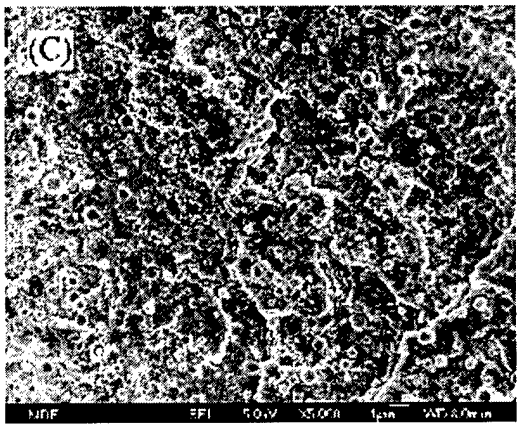

Figure 6.7 SEM micrographs of the fracture surface PA-6-clay-PVDF ternary nanocomposite containing 10 wt% PVDF.

Figure 6.8 shows the SEM micrographs of fracture surface in PA-6-clay-PVDF ternary nanocomposite containing 20 wt% PVDF. Some plastic deformation of the matrix is also observed at the crack initiation stage at location A (Figure 6.8A). The same comment regarding the 10% PVDF composite applies here. What little plastic deformation there is disappears at location B (Figure 6.8B) and C (Figure 6.8C). PVDF particles around 1μm are seen in this figure. These particles are greater than those composites containing 10 wt% PVDF. The trend of increase of PVDF particle size with increasing PVDF content is the same as that reported in literature. It may be that PVDF, which is lower than PA-6 in viscosity, reduces the overall intensity of mixing when the former is present in large amounts. The reduced mixing intensity provided less stress to break up the PVDF into fine particles. Debonding at the PA-6-PVDF interfaces is also observed. Some PVDF particles were also detached from the fracture surface. Some PVDF particles were also fractured from this figure.

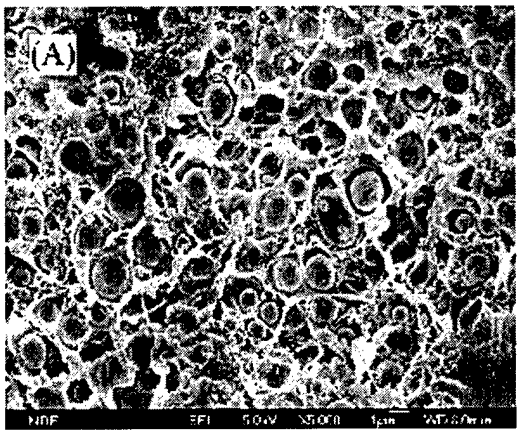

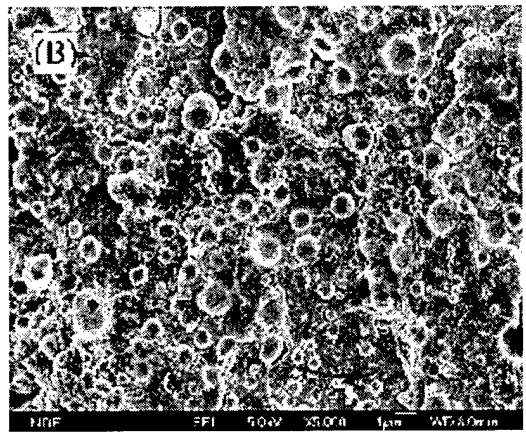

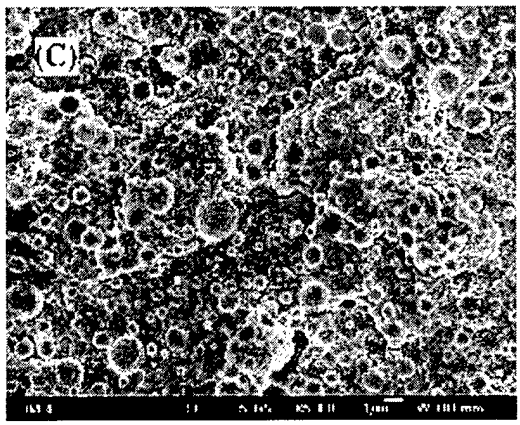

Figure 6.8 SEM micrographs of the fracture surface subject to K_c measurement for PA-6-clay-PVDF nanocomposite containing 20 wt% PVDF.

It was shown that the fracture toughness K_c of the ternary nanocomposites increases with increasing PVDF content. The plastic deformation on the fracture surface suggests that there is extensive voiding around the PVDF particles as well as coalescence when these voids grew. (The deformation *not* visible to SEM may be more important than what *is* visible. This is probably the reason why the toughness seems to go against the trend in the amount of visible surface plastic deformation). The absence of plastically stretched particles on the surface suggests that the debonding took place rather too early. It is also obvious that addition of PVDF particles changed the fracture behaviour of the ternary nanocomposites. The fracture surface of ternary nanocomposites is much coarser than the one of binary nanocomposite without PVDF at the crack propagation stage (locations B and C). Sub-surface microscopy will need to be conducted to further elucidate these features.

It is also noticed that the bridging mechanism is not significant in the system studied. This may be explained by the fact that: (1) the yield stress of PVDF is not low enough, and (2) the interfacial adhesion is not strong enough. However, a further strengthening of interfacial adhesion will definitely lead to a decrease of particle size. The small size of the particles may be disadvantageous for bridging since a crack may jump over them.

iv. SAXS Anaylsis

SAXS study of a fractured sample is shown in figure 6.9. The scattering in the direction perpendicular to the tensile axis exhibits a strong spherical component, indicating that the amount of crazing, if any, should be very small. The strong

spherical scattering intensity compared with the polymer system without PVDF clearly indicates a phase separation of PVDF in PA-6. In the direction parallel to the tensile axis, there is an equatorial scattering component, indicating the existence of micro-cracks. Clearly, the addition of PVDF did not significantly alter the fracture mechanism of the polymer matrix. However the system exhibited better mechanical properties compared with a system consisting of 95% PA-6 and 5% clay. The elongation at break increases 60% and the fracture toughness, Kc, increased about 20%, as discussed in the mechanical property section.

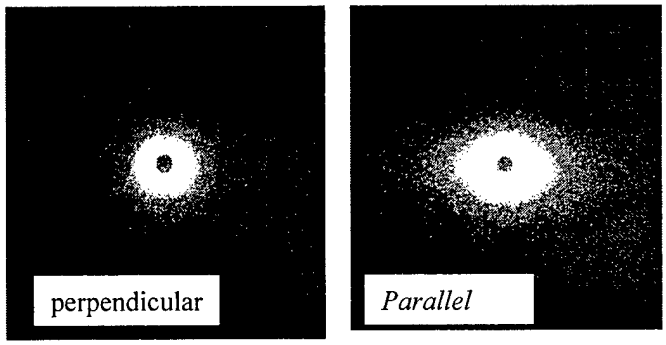

Figure 6.9: SAXA of deformed Nanocomposite

10 wt-% PVDF, 85.5% PA-6 and 4.5% clay

7. Toughening of Silsesquioxane Epoxy Resin

Silesequioxane epoxy (POSS) resin is another polymer system with nano-scale structure in our study. POSS moieties are essentially polyhedral cages composed of Si and O atoms with chemical formula Si_8O_{12}. It has been found that organic-inorganic hybrid polymers made of POSS possess several attractive properties such as increased thermal stability, high glass transition temperature, better flame and heat resistance, and enhancement in moduli and melt strengths. Polymer materials containing POSS have been regarded as structural materials for the next generation. The objective is to study the deformation behavior of POSS based epoxy composites with high modulus. Our ultimate aim is to formulate a strategy to toughen the epoxy system.

i. Experimental

The criterion for materials selection is that the matrix system should have high T_g and good thermal stability along with good processability. Octa cyclohexenyl silsesquioxane epoxide cube (**OC**) from Prof. Laine's group at Michigan was selected as a candidate for this study while diaminodiphenyl methane (**DDM**) from Alfa Aesar was chosen as curing agent as shown in the figure.

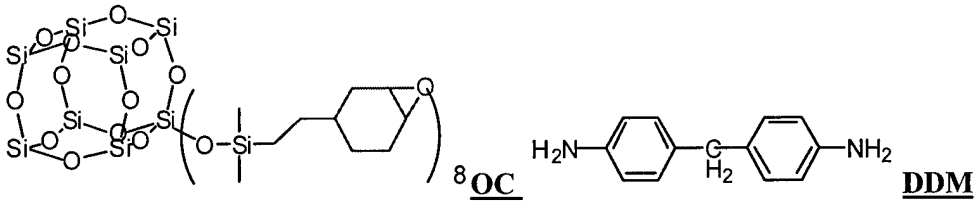

Scheme 1: chemical structure of OC and DDM

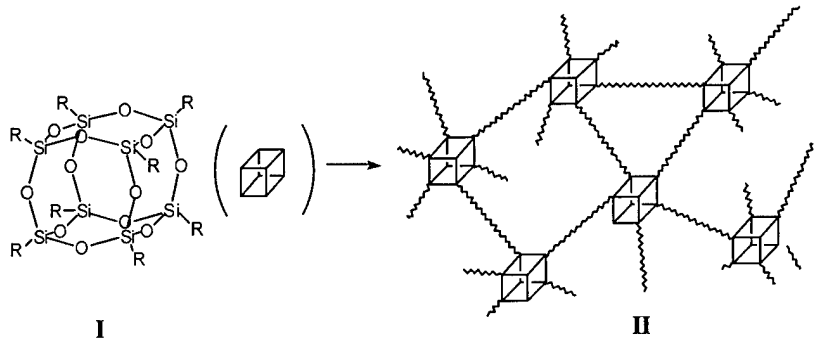

Scheme 2: formation of the nanocomposites from cubic silsesquioxane: OC/DDM structure at N = 1.0

ii. Effect of DDM Concentration

The OC/DDM composite properties were well studied in previous research conducted in Laine's group. Formulation variable N is defined as follows;

$$N = \frac{\text{Number of amine groups in DDM}}{\text{Number of epoxy rings in } OC}$$

Thus, when N = 1, there are equal numbers of NH_2 groups and epoxy rings in the sample mixture. A conventional stoichiometric ratio of 2 moles of amine to 1 mole of epoxy would occur for N=0.5. Their elastic modulus, fracture toughness and DMA results are presented in Figure 7.1 and 7.2 (from previous study). The modulus increases with the increase in DDM content and can reach over 3 GPa, while fracture toughness remains between 0.4 ~ 0.6 MPa.m$^{1/2}$. In the following study, N = 1.0 was selected since the nano-network structure can be well defined at this formulation. This OC/DDM loses 5 % mass at 415° C in TGA under N_2 at 5° C/min ramp.

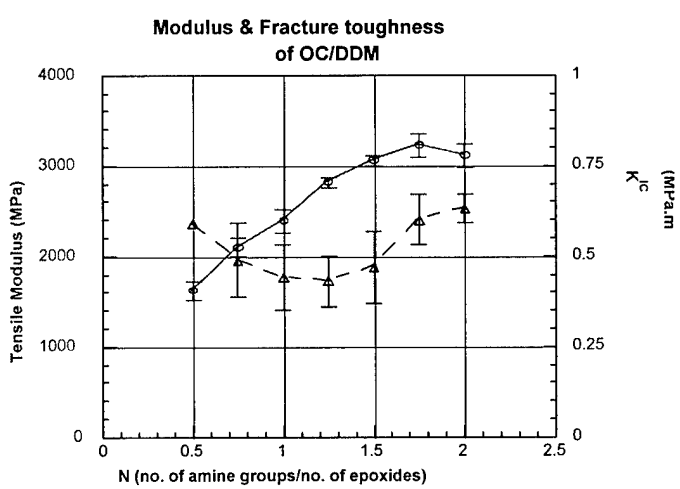

Figure 7.1. tensile modulus and fracture toughness of OC/DDM

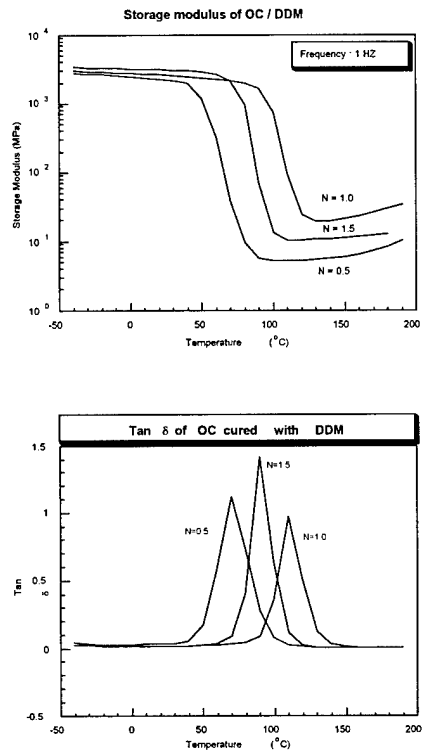

Figure 7.2. DAM results of OC/DDM

iii. Effect of Curing Condition

The curing condition influences the glass transition temperature of the resulting epoxy system. The cure condition employed for the above OC/DDM matrix was 10 hrs at 150° C which leads to Tg of ~ 110° C at N = 1. When the epoxy system was cured at high temperature for a longer time the resulting epoxy matrix exhibits a higher T_g and a higher rubbery state modulus as shown in figure 7.3. All OC/DDM prepared under various cure conditions show 5 % mass loss temperatures at 412 ± 5 ° C. The Vicker hardness test was performed on OC/DDM as a rough measure of the mechanical strength of these materials. Loading mass and loading time with Vicker hardness numbers are shown in table 7.1. Water absorption of the composite was also tested. Thin sliced sections were kept in water at 50° C and their weight changes were monitored for 7 days. It was determined that the maximum water uptake of pure OC/DDM was about 1 wt % and most of its weight was gained in 1 day.

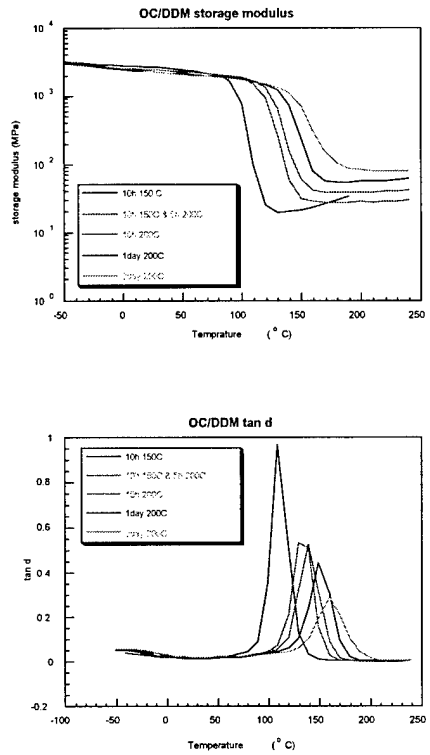

Figure 7.3. DMA results of OC/DDM at various cure conditions

Table 7.1. Vicker hardness test of OC/DDM at N = 1.0

	30 sec			20 sec		
500 g	227.9 ± 1.7	235.5 ± 2.0	**17.3 ± 0.3**	227.6 ± 1.4	234.5 ± 4.0	**17.4 ± 0.3**
100 g	104.1 ± 2.8	102.6 ± 4.5	**17.4 ± 1.0**	103.9 ± 2.4	106.2 ± 1.3	**16.8 ± 1.3**

iv. Deformation of OC/DDM Matrix

Surface indentations with a diamond stylus and optical microscopy (OM) was used to characterize the deformation behaviour of the OC/DDM matrix, primarily for the purpose of determining if these materials are capable of deforming in plastic shear. Initially, an arbitrary force was applied by hand to make an indentation. OM images of the sample cross-section are shown in Figure 7.4.1 to 7.4.3. These images reveal not only a permanent indentation but also a crack beneath the tip of the indentation. Birefringence in Figure 7.4.1 shows that both plastic and elastic deformations are possible in this matrix. To release the elastic deformation from the indentation, half of the cross section was cut off and OM images of a quarter of the indentation were taken as shown in Figure 7.4.2 and 7.4.3. In these Figures, birefringence is still vivid, indicating that the capacity for plastic deformation is significant in the matrix.

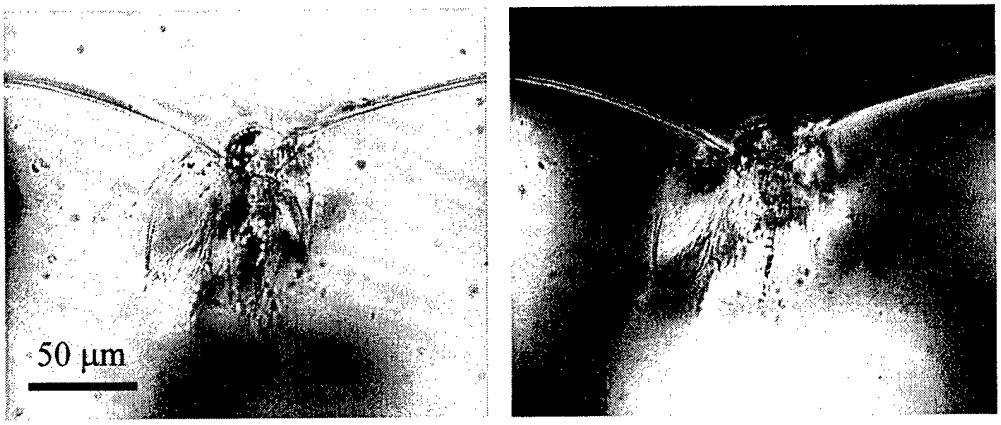

Figure 7.4.1. Indentation by a diamond stylus, arbitrary load, x 400

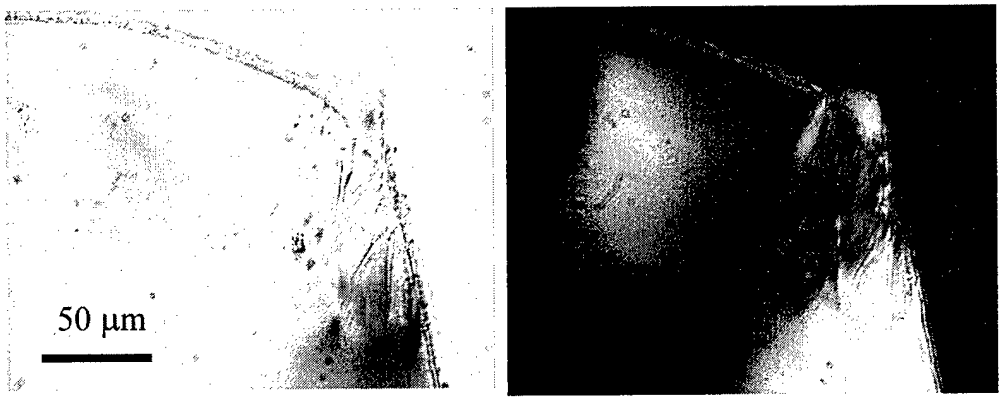

Figure 7.4.2. Indentation by a diamond stylus, arbitrary load, x 400

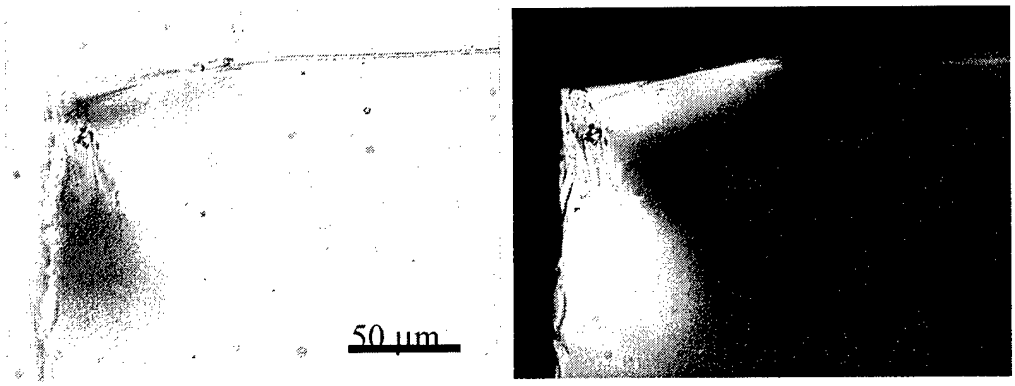

Figure 7.4.3. Indentation by a diamond stylus, arbitrary load, x 400

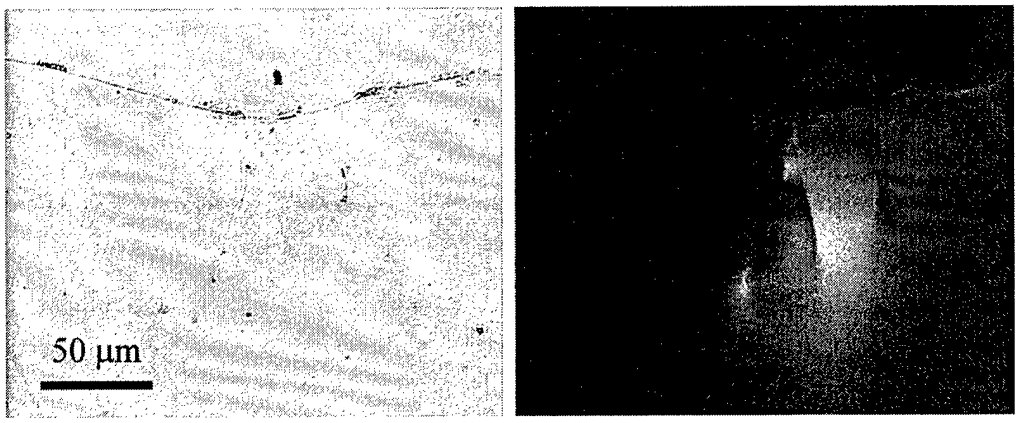

Figure 7.4.4. Indentation by a diamond stylus, 1000g load, x 400

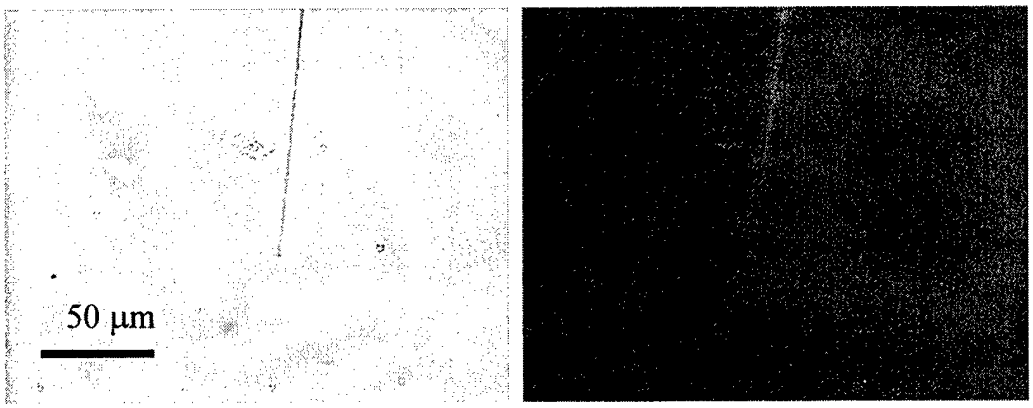

Figure 7.4.5. A crack tip made by 4-point bending, x 400

This argument is supported when constant loading of 1000 g was applied. Figure 7.4.4 shows that an indentation was made without generating many cracks. Only 3 crack lines are observed. Therefore, it is clear that OC/DDM can undergo plastic deformation and a conventional toughening technique may be appropriate. Unfortunately, a crack made by 4-point bending test (Figure 7.4.5) did not show any clear birefringence in OM.

v. Toughening of OC/DDM Using Core-Shell Rubber

It is clear that the OC/DDM system is brittle but can undergo plastic deformation. Incorporation of rubber particle may be a good strategy to improve the toughness of the system as cavitation and shear yield due to inclusion of rubber particles would dissipate fracture energy and results in a tougher composite. OC was originally mixed with core shell rubber (CSR) (from Prof. Sue's group in Texas A & M) in methylethylketone (MEK) solution. MEK was removed by vacuum drying. The fraction of CSR in OC was 20 wt-%. This OC/CSR was then diluted with pure OC to 4 % and cured with DDM for 1 day at 200° C. In curing, two different methods were tested; (1) 4 % OC and DDM were dissolved in MEK and then MEK was removed by vacuum drying at 200° C. followed by 1 day curing under N_2 (**solution process**). (2) 4 % OC and DDM were melted together at 200° C and mixed by stirring bar for several minutes, followed by 1 day curing under N_2 (**melt process**).

a Deformation behavior of OC/DDM/CSR Composites

Figure 7.5.1 shows that an indentation without a crack was made on the surface of the specimen prepared in the solution process and its birefringence was significant. Occasionally, small damages beneath the indentation tip were observed as shown in Figure 7.5.2. In cross section images of composites prepared by the melt process (Figure 7.5.3), rough textures were observed indicating that mixing was not complete or efficient. Therefore, for the coming study, only solution study was used. In all cases, no major segregation of CSR from matrix visible to OM was found.

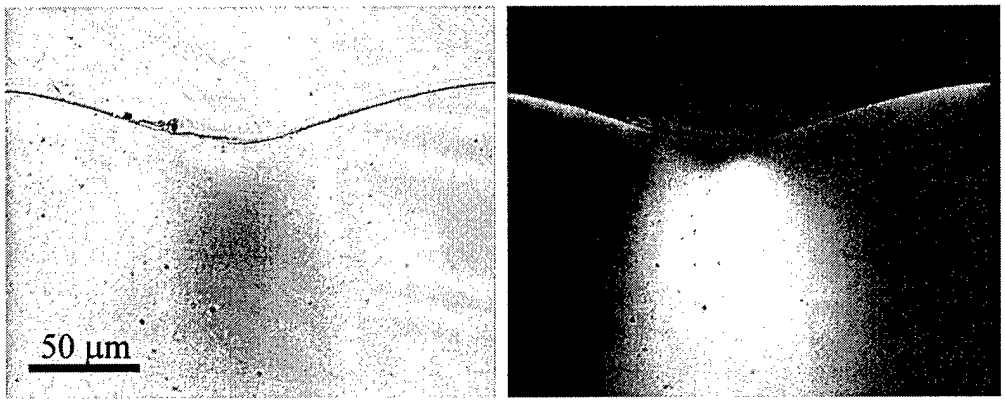

Figure 7.5.1. Indentation by diamond stylus, solution process, 4 % CSR, x 400

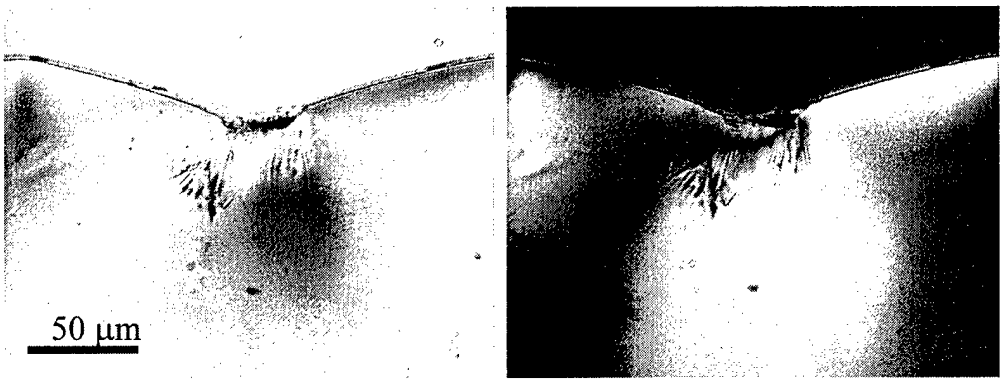

Figure 7.5.2. Indentation by diamond stylus, solution process, 4 % CSR, x 400

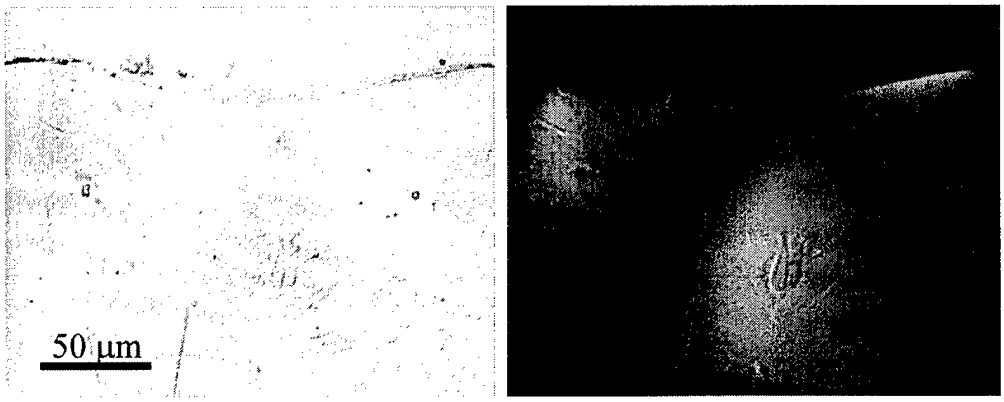

Figure 7.5.3. diamond stylus, melt process, 4 % CSR. x 400

b. Thermal Mechanical Property of OC/DDM/CSR

TGA under N_2 at 5° C/min test shows no apparent decrease in 5 % mass loss temperature in composites as shown in figure 7.6. But, the differences are found in char yields after they were burned at 1000° C. Char yield for OC/DDM was higher than 4 % or 8 % CSR loaded OC/DDM. However, this difference was minimal between 4 % and 8 % CSR composites.

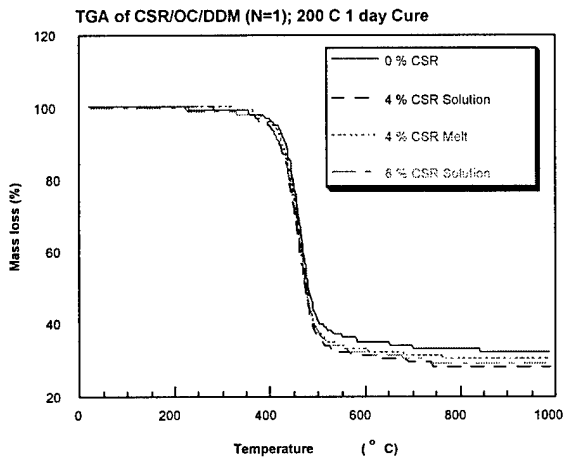

Figure 7.6. TGA of OC/DDM/CSR composites

No significant changes in storage modulus and in tan δ profiles were found as shown in Figure 7.7. All of the tested composites exhibited Tg's of ~ 150° C and rubbery state modulus of ~ 65 MPa, indicating that the incorporation of CSR in OC/DDM does not affect the glass transition and modulus of the matrx.

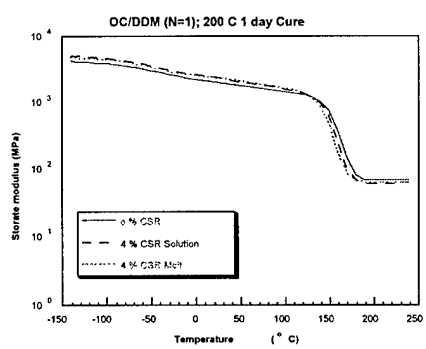

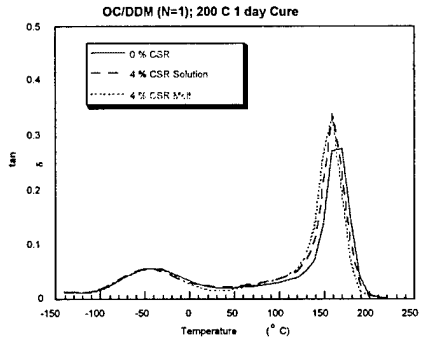

Figure 7.7. DMA results of OC/DDM/CSR composites

c. *Compression Test*

Compression tests were performed on cylindrical shaped composites and the stress-strain curves are shown in Figure 7.8. Unfortunately, because of the low load cell capacity, the test had to be stopped at strain of ~ 0.1. However, even based on these results, it is clear that the initial linear elastic deformation turns into the plastic deformation. But the difference between unloaded and CSR loaded composites cannot be identified clearly. This test will be resumed with a different load cell in the near future.

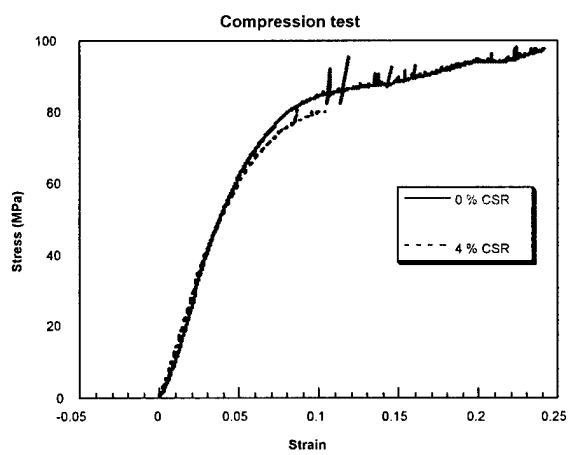

Figure 7.8. Stress-strain curves of compression test

d. *Fracture Toughness*

The fracture toughness, K_{IC}, was characterized using 3 point bending test on unloaded and CSR loaded OC/DDM composites. The increase of fracture toughness seems rather minimal (~10%) as shown in table 7.2. It is necessary to test higher CSR loading composites.

Table 7.2. Fracture toughness values of OC/DDM/CSR composites

	KIC ($MPa.m^{1/2}$)
0 % CSR	0.598 ± 0.012
4 % CSR	0.661 ± 0.047

e. SEM of CSR modified material

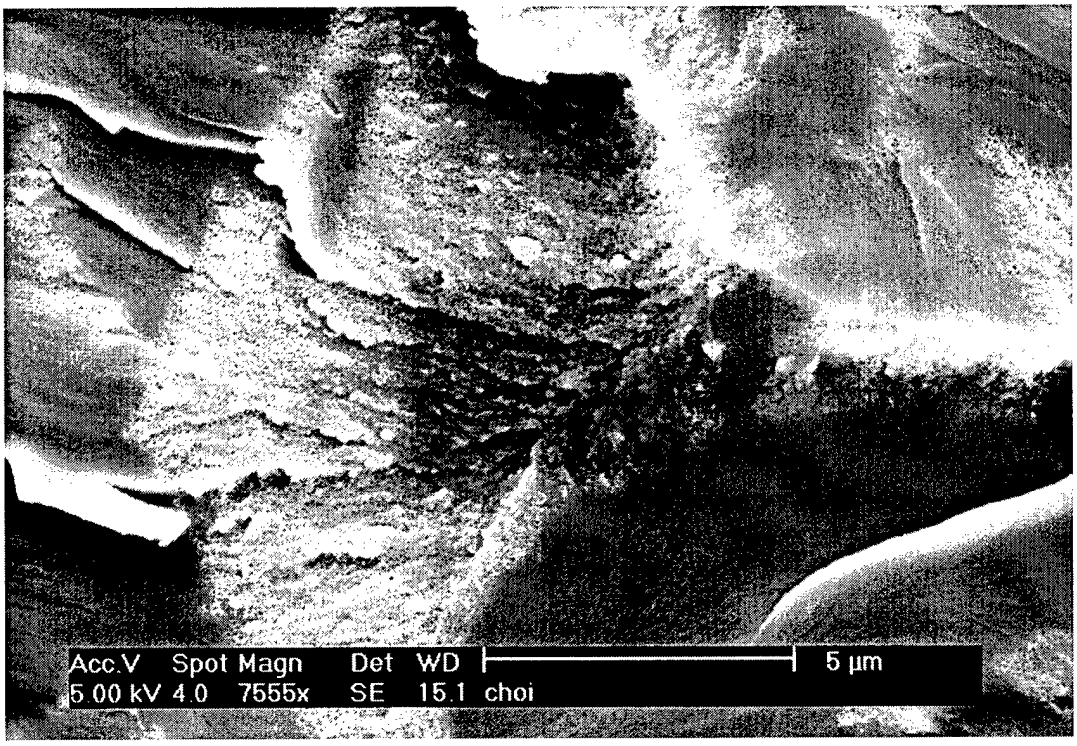

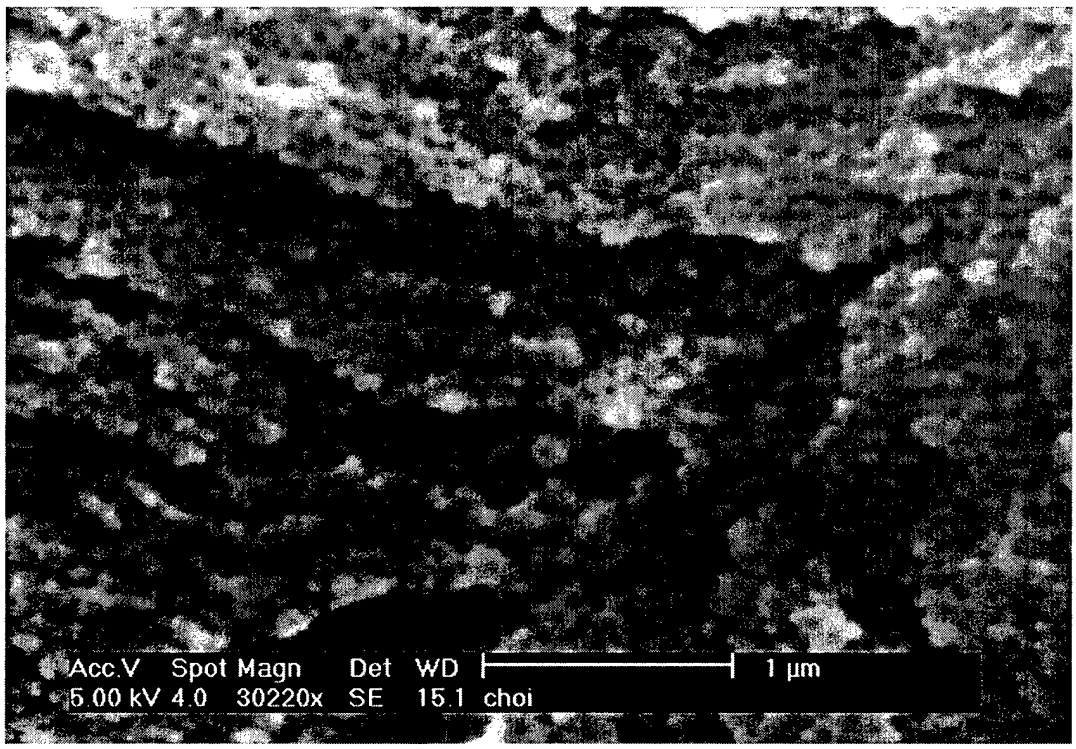

The upper micrograph suggests that phase segregation had occurred. This may have been because the original 20 % CSR loaded into the OC matrix was diluted with pure OC later, and the mixing was not perfect. Nevertheless, K_{IC} improved from 0.6 to 0.95.

8. Conclusions

The embrittlement of PA-6 nano-clay composites is mainly due to micro-cracking followed by global fracture. The toughening by bridging approach is somewhat effective. PVDF shows no evidence of plastic deformation, but good adhesion.

Silsesquioxane epoxy based on octa-cyclohexenyl silsesquioxane epoxide cubes (OC) and diaminodiphenyl methane (DDM) (from Alfa Aesar) is brittle but some extent of plastic deformation was observed. Toughening through addition of core-shell rubber particle (up to 4 wt-%) however seems not very effective. Further study may involve high concentration of CSR.

9. Further Research

The research presented in this progress report put forward some potential areas for further investigations. Firstly, we studied strategies to improve the mechanical property of the composite. The embrittlement mechanism for the PA-6-nanocomposite is found to be mainly due to micro-cracking followed by global fracture. One way to improve the mechanical property of the composites is to use the bridging approach. This approach has been proven in this research to be somewhat effective. Another approach is to induce massive crazing. As has been demonstrated

in PA-6-nanoclay composite containing 2.5% clay, massive crazing absorbs fracture energy and leads to a tougher composite. In the next step, rubber particles will be introduced into the PA-6-nanoclay composite system to facilitate massive crazes. The relation between craze concentration and toughness of the composite will be studied.

Secondly, we performed quantitatively analyses of the craze concentration using SAXS. Crazing is an important factor influencing the fracture behaviour of polymers. The research described in this progress report has laid out a framework for quantitatively analysing crazing using the SAXS method. In the next step, the effect of clay and toughening agent on craze concentration and the consequent deformation behaviour will be studied quantitatively.

Thirdly, we investigated the deformation behaviour and fracture mechanism of epoxy nanoclay composites and formulated strategies for toughening epoxy nanoclay composites. The research described in this progress report mainly focuses on a semi-crystalline polymer material: PA-6. In the next step we will study an amorphous thermoset system, viz., epoxy nanoclay composites using various techniques used in this research.